Cell Marker Accordion: interpretable single-cell and spatial omics annotation in health and disease

Emma Busarello[1,*,✉], Giulia Biancon[2,3,*], Ilaria Cimignolo[1], Fabio Lauria[4], Zuhairia Ibnat[1], Christian Ramirez[1], Gabriele Tomè[1,4], Marianna Ciuffreda[1], Giorgia Bucciarelli[1], Alessandro Pilli[1], Stefano Maria Marino[1], Vittorio Bontempi[5], Federica Ress[6], Kristin R. Aass[7], Jennifer VanOudenhove[2], Luca Tiberi[6], Maria Caterina Mione[5], Therese Standal[7], Paolo Macchi[8], Gabriella Viero[4], Stephanie Halene[2,9,✉] and Toma Tebaldi[1,2,✉]

1 Laboratory of RNA and Disease Data Science, Department of Cellular, Computational and Integrative Biology (CIBIO), University of Trento, Trento, Italy

2 Section of Hematology, Department of Internal Medicine, Yale Comprehensive Cancer Center, Yale University School of Medicine, New Haven, CT, USA

3 Hematology Unit, Fondazione IRCCS Ca' Granda Ospedale Maggiore Policlinico, Milan, Italy

4 Institute of Biophysics, CNR Unit at Trento, Italy

5 Laboratory of Experimental Cancer Biology, Department of Cellular, Computational and Integrative Biology (CIBIO), University of Trento, Trento, Italy

6 *Armenise-Harvard Laboratory of Brain Disorders and Cancer, Department of Cellular, Computational and Integrative Biology (CIBIO), University of Trento, Trento, Italy*

7 Department of Clinical and Molecular Medicine, Norwegian University of Science and Technology (NTNU), Trondheim, Norway.

8 Laboratory of Molecular and Cellular Neurobiology, Department of Cellular, Computational and Integrative Biology (CIBIO), University of Trento, Trento, Italy

9 Department of Pathology, Yale University School of Medicine, New Haven, CT, USA

** Equally contributed*

Correspondence to: emma.busarello@unitn.it, stephanie.halene@yale.edu, toma.tebaldi@unitn.it

Abstract

Single-cell technologies offer a unique opportunity to explore cellular heterogeneity in health and disease. However, reliable identification of cell types and states represents a bottleneck. Available databases and analysis tools employ dissimilar markers, leading to inconsistent annotations and poor interpretability. Furthermore, current tools focus mostly on physiological cell types, limiting their applicability to disease.

We developed the Cell Marker Accordion, a user-friendly platform providing automatic annotation and unmatched biological interpretation of single-cell populations, based on consistency weighted markers. We validated our approach on multiple single-cell and spatial datasets from different human and murine tissues, improving annotation accuracy in all cases. Moreover, we show that the Cell Marker Accordion can identify disease-critical cells and pathological processes, extracting potential biomarkers in a wide variety of disease contexts.

The breadth of these applications elevates the Cell Marker Accordion as a fast, flexible, faithful and standardized tool to annotate and interpret single-cell and spatial populations in studying physiology and disease.

Introduction

Single-cell RNA sequencing (scRNA-seq) characterizes the transcriptome of each cell in large populations. This high-throughput approach is the ideal choice to reveal the heterogeneous landscape of normal and aberrant cell differentiation processes. It enables the study of cells with diverse properties, including varying self-renewal capacity, multipotent potential, and high plasticity, which are critical in infections, immune responses, and disease pathogenesis[1–3]. Spatial omics further contribute by adding architectural context, revealing how cells are organized within tissues and how this influences their function[4,5].

With the enormous opportunities offered by single-cell technologies, a new set of challenges is rapidly emerging in data analysis and interpretation. Accurate and reliable annotation of cell types is key to deriving faithful biological conclusions. Robustness in identifying cell types is an essential prerequisite to discern disease-critical cells, characterized by aberrant cell states responsible for disease initiation, progression and therapy resistance[6]. In addition, measuring the single-cell activity of gene signatures or modules associated with pathologically relevant pathways is fundamental to unravelling pathogenic mechanisms in aberrant cells[7] and discovering potential disease biomarkers[8].

Identification of cell populations within single-cell data can be executed manually or automatically[9]. Manual annotation, based on the investigator's knowledge or derived from published literature, is generally subjective and often non-reproducible due to lack of standardization. Many computational tools perform automatic annotation by correlating reference expression data or transferring labels from other single-cell datasets[10–13]. These approaches require reliable transcriptome profiles of purified cells or high-quality annotated single-cell data[14]. However, such reference datasets are not readily available, especially for pathological samples; they can lack the cell populations of interest and might be susceptible to technical specificities such as platform or sequencing strategy[15]. Alternatively, automatic annotation can be achieved by employing predefined sets of cell marker genes[16–18]. Many current tools require the user to provide a collection of markers, a process prone to bias[12,17,19].

We show that currently available gene marker databases are extremely heterogeneous, contain different marker sets for the same cell type, and employ a non-standard nomenclature and classification, thus leading to inconsistent annotation of cell populations in scRNA-seq and spatial data, and poor interpretability of results. Furthermore, current tools and resources focus mostly on physiological cell types, limiting the identification of disease-critical cells. To address these issues and improve the interpretation of normal and aberrant cell types in single-cell and spatial data, we developed the Cell Marker Accordion, an easily accessible and well-documented platform constituted by an interactive R Shiny web application requiring no programming skills and an R package.

The Cell Marker Accordion database is built upon multiple published databases of human and mouse gene markers for cell types (**Supplementary Data 1**) (both general and tissue-specific), standard collections of widely used cell sorting markers and literature-based marker genes associated with disease-critical cells in multiple pathologies, including liquid and solid tumors. The Accordion database allows marker genes to be weighted not only by their specificity but also by their evidence consistency score, measuring the agreement of different annotation sources. The Cell Marker Accordion web interface permits to explore the integrated collection of marker genes and to easily browse hierarchies of cell types following the Cell Ontology structure to obtain the desired level of resolution with tissue specificity.

The Cell Marker Accordion R package allows to automatically annotate healthy and aberrant populations in single-cell datasets from multiple tissues, exploiting positive and negative markers from either the built-in Accordion database or any gene signature of interest provided by the user. Genes, cell types or pathways that mostly influence annotation results can be easily accessed and visualized to allow the transparent interpretation of results.

We benchmarked the Cell Marker Accordion on multiple single-cell and spatial omics datasets, using surface markers and expert-based annotation as the ground truth. In all cases, we significantly improved the annotation accuracy with respect to existing annotation tools. Moreover, we show that the Cell Marker Accordion can be used to identify pathological processes and disease-critical cells: leukemia cell subtypes, including therapy-resistant cells, in acute myeloid leukemia patients[20,21]; neoplastic plasma cells in multiple myeloma samples[22,23]; malignant subpopulations in glioblastoma and lung adenocarcinoma patients[24,25]; cell type alterations driven by pathologically relevant mutations in myelodysplastic syndromes[26,27]; activation of innate immunity pathways in bone marrow from mice with Mettl3 deletion or treated with METTL3 inhibitors[28,29].

The Cell Marker Accordion is a fast, user-friendly, flexible and comprehensive tool that improves the annotation and interpretation of both physiological and pathological cell populations with single-cell resolution.

Results

Widespread heterogeneity across annotation sources leads to inconsistent cell type annotation

To unravel information discrepancies across currently available gene marker databases, we automatically annotated a published scRNA-seq dataset of human bone marrow[30], extracting marker genes from CellMarker2.0[31] and Panglao DB[32], two of the most comprehensive databases for cell type markers (**Fig.1A,** see **Methods**). Cell type annotation was often inconsistent between the two sources, showing divergent cell types assigned to the same cluster (for example, “hematopoietic progenitor cell” and “anterior pituitary gland cell”) or different nomenclature (for example “Natural killer cell” and “NK cells”). We unfolded very high discrepancies in marker genes utilized by these resources, with a maximum Jaccard similarity index of 0.23 between matching cell types (**Fig.1B**).

To extend this initial observation, we systematically explored the heterogeneity of seven available marker gene databases over common cell types[31–37] (see **Methods**). The comparison showed low consistency between databases, with an average Jaccard similarity index of 0.08 and a maximum of 0.13 (**Fig.1C**). These results show that different marker gene databases inevitably lead to inconsistent interpretations of the biological meaning of single-cell data and raise concerns with profound consequences for data mining.

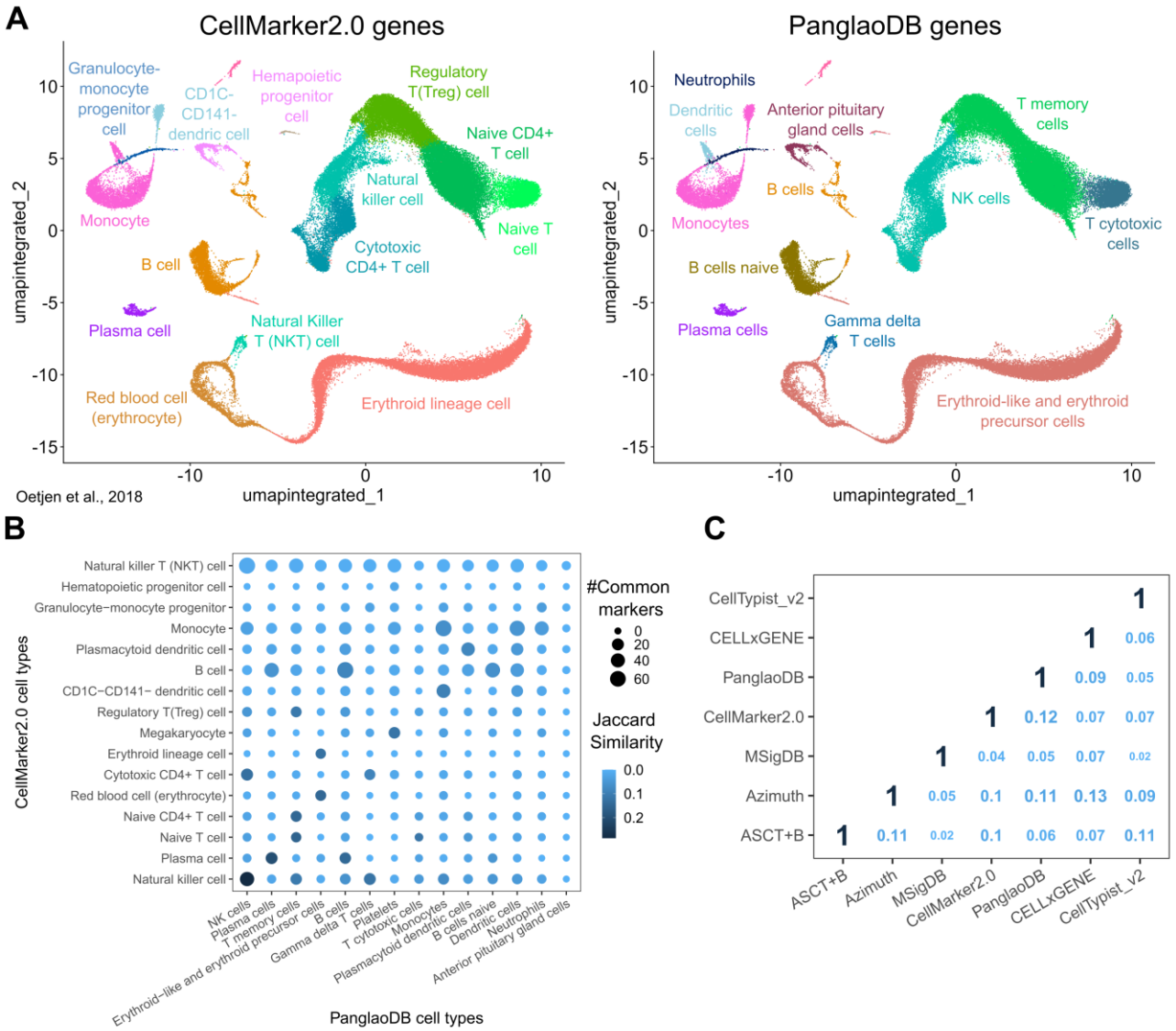

Fig.1: Heterogeneity in marker gene databases leads to inconsistent single-cell annotations. ***A*** *Cell type identification by automatic annotation with ScType[38] in a published bone marrow dataset[30] , using markers from CellMarker2.0 (left) and PanglaoDB (right) as input.* ***B*** *Overlap between marker genes from CellMarker2.0 (y-axis) and PanglaoDB (x-axis). The dot color represents the Jaccard similarity index, and the dot size indicates the number of common markers in each cell type pair.* ***C*** *Comparison of cell type markers among seven published databases. The numbers indicate the average Jaccard similarity index between each database pair, calculated using all common cell types.*

The Cell Marker Accordion: a user-friendly platform for the annotation and interpretation of single-cell populations

To address the need of robust and reproducible identification of cell types in single-cell datasets, we developed the Cell Marker Accordion, comprising a gene marker database, an R shiny web app and an R package to automatically annotate and interpret single-cell populations.

We built the Cell Marker Accordion database by integrating 23 marker gene databases and cell sorting marker sources (**Supplementary Data 1**), distinguishing positive from negative markers (**Fig.2A**). Standardization was achieved by mapping the initial cell type nomenclature to the Cell

Ontology terms[39] and tissue names to the Uber-anatomy ontology (Uberon) terms[40]. Next, via database integration, we obtained a comprehensive set of cell-type specific marker genes, human and murine, in hundreds of tissues. Importantly, in the Cell Marker Accordion database, genes are weighted by their specificity score (SPs), indicating whether a gene is a marker for different cell types, and by their evidence consistency score (ECs), measuring the agreement of different annotation sources (see **Methods**).

The intuitive and interactive Accordion Shiny web interface permits easy retrieval of marker genes associated with input cell types and *vice versa*, starting from a list of candidate genes to obtain the matching cell types (**Fig.2B right**). Hierarchies of cell types can be easily browsed following the Cell Ontology structure to select and obtain the desired level of resolution in the markers. Users can upload a custom sets of genes to either update the repository or perform cell type marker enrichment analysis, with no need for programming skills.

Finally, the Cell Marker Accordion R package allows to automatically annotate cell populations based on the built-in database, with the considerable advantage of weighting the markers according to their evidence consistency and specificity scores (**Fig.2B left and Supplementary Fig.1**). The automatic annotation can be easily integrated into a Seurat analysis workflow[34], requiring as input only the count matrix or a Seurat object. Built-in lists of positive and negative cell cycle markers can be used to assign the appropriate cell cycle phase to each cell or to evaluate quiescence. Any annotation procedure can be easily enhanced by including custom gene lists associated with cell types, specific pathways or signatures of interest. Importantly, with respect to other tools, the Cell Marker Accordion implements novel options to explore annotation results by providing the top marker genes that most significantly determine the final annotation. The diversity or similarity of the top cell types competing for the same annotation can be evaluated by inspecting their position along the Cell Ontology tree (**Supplementary Fig.2**).

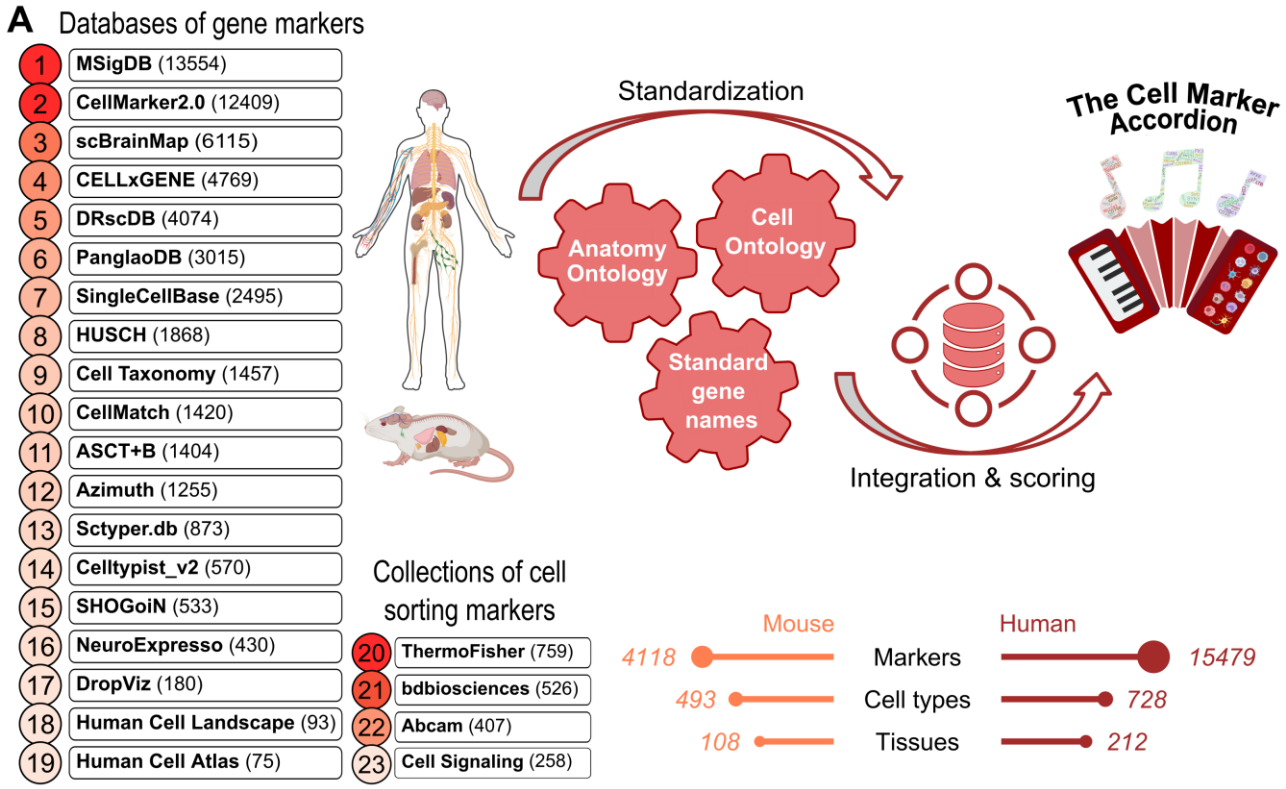
A
Databases of gene markers
1 MSigDB (13554)
2 CellMarker2.0 (12409)
3 scBrainMap (6115)
4 CELLxGENE (4769)
5 DRscDB (4074)
6 PanglaoDB (3015)
7 SingleCellBase (2495)
8 HUSCH (1868)
9 Cell Taxonomy (1457)
10 CellMatch (1420)
11 ASCT+B (1404)
12 Azimuth (1255)
13 Sctyper.db (873)
14 Celltypist_v2 (570)
15 SHOGoiN (533)
16 NeuroExpresso (430)
17 DropViz (180)
18 Human Cell Landscape (93)
19 Human Cell Atlas (75)
Standardization
Anatomy Ontology
Cell Ontology
Standard gene names
Integration & scoring
The Cell Marker Accordion
Collections of cell sorting markers
20 ThermoFisher (759)
21 bdbiosciences (526)
22 Abcam (407)
23 Cell Signaling (258)
Mouse
Human
4118 Markers 15479
493 Cell types 728
108 Tissues 212

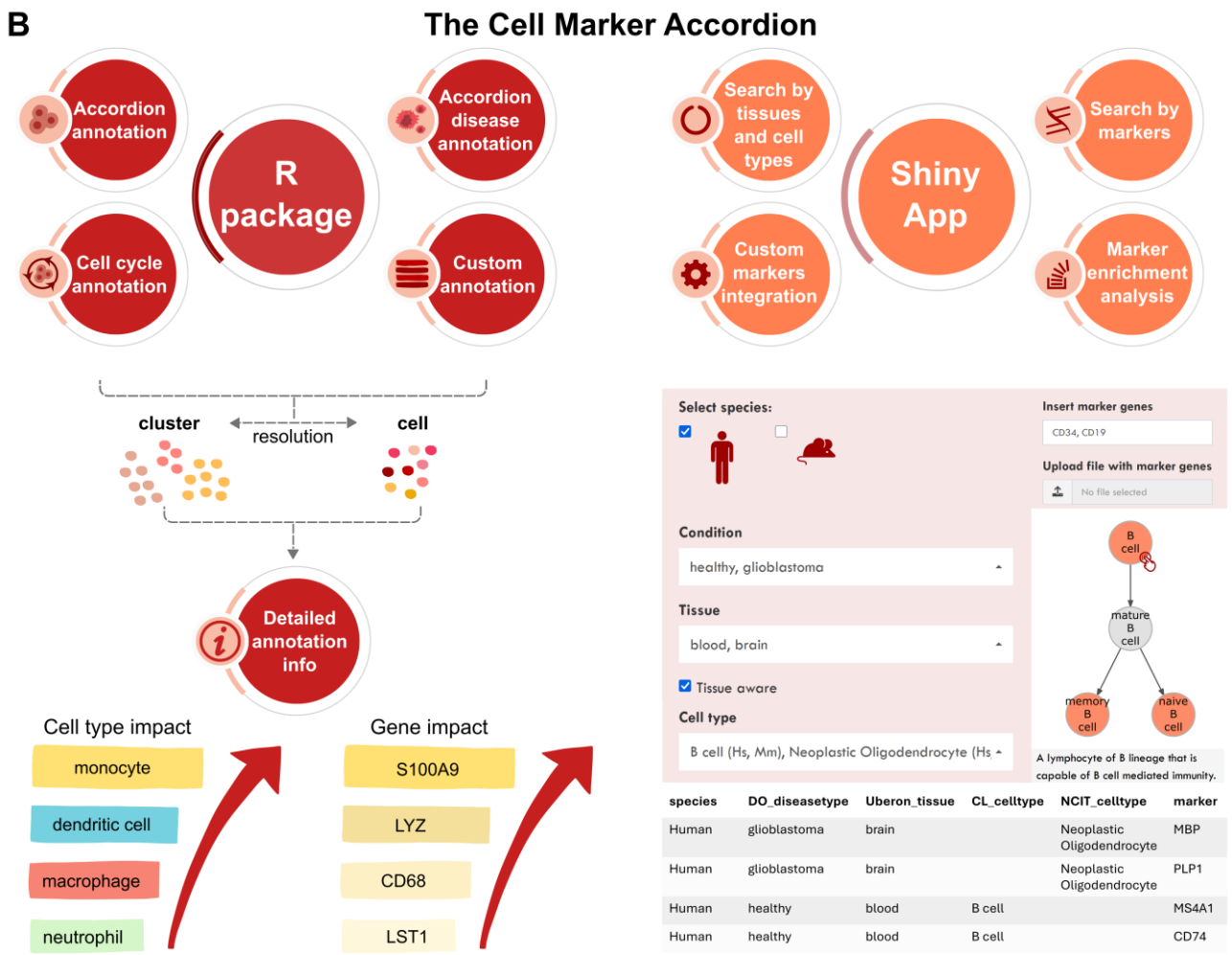
B
The Cell Marker Accordion
Accordion annotation
Cell cycle annotation
R package
Accordion disease annotation
Custom annotation
Search by tissues and cell types
Custom markers integration
Shiny App
Search by markers
Marker enrichment analysis
cluster
resolution
cell
Detailed annotation info
Cell type impact
monocyte
dendritic cell
macrophage
neutrophil
Gene impact
S100A9
LYZ
CD68
LST1
Select species:
Insert marker genes
CD34, CD19
Upload file with marker genes
No file selected
Condition
healthy, glioblastoma
Tissue
blood, brain
Tissue aware
Cell type
B cell (Hs, Mm), Neoplastic Oligodendrocyte (Hs
B cell
mature B cell
memory B cell
naive B cell
A lymphocyte of B lineage that is capable of B cell mediated immunity.
species DO_diseasetype Uberon_tissue CL_celltype NCIT_celltype marker
Human glioblastoma brain Neoplastic Oligodendrocyte MBP
Human glioblastoma brain Neoplastic Oligodendrocyte PLP1
Human healthy blood B cell MS4A1
Human healthy blood B cell CD74

***Fig.2: The Cell Marker Accordion: a user-friendly platform for annotating and interpreting single-cell populations**. **A** Workflow for building the Cell Marker Accordion database. Sources are ranked according to their initial number of markers. The resulting numbers of human and murine markers, cell types and tissues are reported. Mouse and human illustrations created in BioRender. Tebaldi, T. (2025) https://BioRender.com/x09w717. **B** Overview of the main functionalities of the Cell Marker Accordion R package and Shiny app.*

The Cell Marker Accordion improves the annotation of cell types in complex single-cell and spatial multi-omics

To validate the Cell Marker Accordion, we undertook a benchmark study to compare its annotation performance against five other automatic tools based on markers: ScType[38], SCINA[19], clustifyR[12], scCATCH[41] and scSorter[17] (described in **Supplementary Data 2**), using multiple published human and murine datasets across different tissues and platforms (**Fig.3, Supplementary Fig.3 and 4**).

First, we exploited a 94655 cells single-cell RNA-seq dataset[42] acquired from fluorescent antibody-sorted (FACS) blood cells, based on 15 cell surface markers and resulting in 10 different populations, separately profiled, that we used as ground truth (**Fig.3A**). Compared to all the other tools[12,17,19,38,41] (see **Methods**), the Cell Marker Accordion shows improved cell type assignment (**Fig.3B**) and lower running time (**Fig.3C**), making it suitable for larger datasets and real-world applications. Furthermore, we provide unique visualizations to boost the interpretation of results in terms of cell types competing for the final annotation (**Fig.3D)**, together with their similarity based on the Cell Ontology hierarchy (**Fig.3E**) and the top influential marker genes (**Fig.3F**).

To extend our benchmark, we selected two human bone marrow datasets, obtained via similar multi-omics methods (CITE-seq and AbSeq), that simultaneously captured RNA and protein expressions[43,44]. In the first case, 25 barcoded antibodies were used to quantify surface proteins and identify 14 different cell types in 30602 total cells (**Supplementary Fig.3A**). The second dataset comprised 13159 cells, classified into 24 different cell types according to the expression of 97 barcoded antibodies (**Supplementary Fig.3B**). We considered surface markers as the ground truth to evaluate and compare annotation results. Additionally, we analyzed five single-cell RNA-seq datasets derived from different tissues: immune system (https://www.ebi.ac.uk/gxa/sc/experiments/E-HCAD-4), pancreas[45] , liver[46], lung[47] and kidney[45] all of which featured expert-curated cell type annotations serving as the ground truth (**Supplementary Fig. 3C** and **Supplementary Fig.4A-D**). Notably, in all cases, the Cell Marker Accordion showed improved annotation performances, with an average increase of approximately 23% with respect to the other tools (**Fig.3G, Supplementary Data 3** for a breakdown of the results in each cell type).

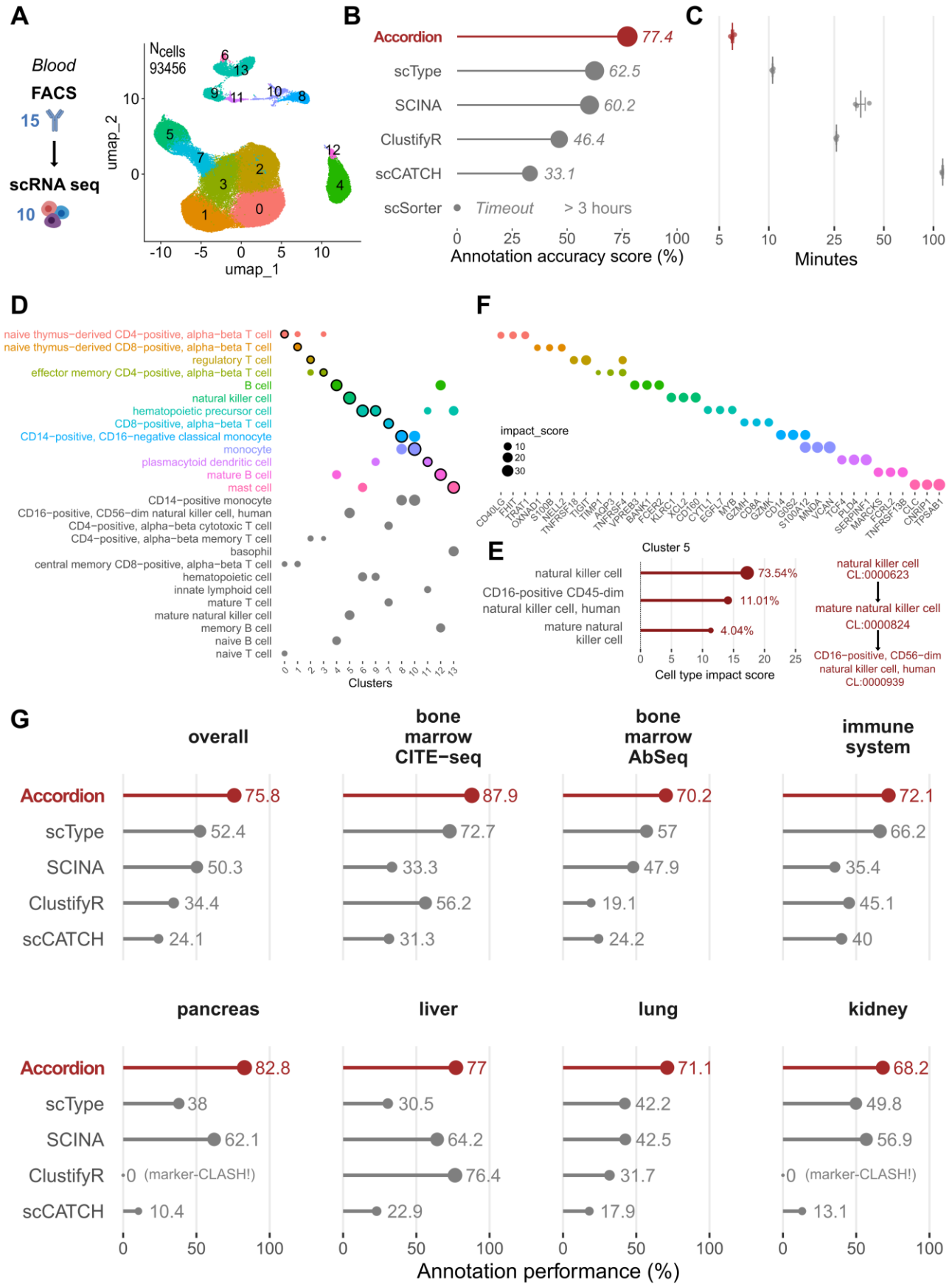
A
Blood
FACS
15
scRNA seq
10
Ncells
93456
umap_2
umap_1
B
Accordion 77.4
scType 62.5
SCINA 60.2
ClustifyR 46.4
scCATCH 33.1
scSorter Timeout > 3 hours
Annotation accuracy score (%)
C
Minutes
D
naive thymus−derived CD4−positive, alpha−beta T cell
naive thymus−derived CD8−positive, alpha−beta T cell
regulatory T cell
effector memory CD4−positive, alpha−beta T cell
B cell
natural killer cell
hematopoietic precursor cell
CD8−positive, alpha−beta T cell
CD14−positive, CD16−negative classical monocyte
monocyte
plasmacytoid dendritic cell
mature B cell
mast cell
CD14−positive monocyte
CD16−positive, CD56−dim natural killer cell, human
CD4−positive, alpha−beta cytotoxic T cell
CD4−positive, alpha−beta memory T cell
basophil
central memory CD8−positive, alpha−beta T cell
hematopoietic cell
innate lymphoid cell
mature T cell
mature natural killer cell
memory B cell
naive B cell
naive T cell
Clusters
F
impact_score
10
20
30
CD40LG EHHT TRAT1 OXNAD1 S100B NELL2 TNFRSF18 TIGIT TIMP1 AQP3 TNFRSF4 VPREB3 BANK1 FCER2 KLRC1 XCL2 CD160 CYTL1 EGFL7 MYB GZMH CD8A GZMK CD14 G0S2 S100A12 MNDA VCAN TCF4 PLD4 SERPINF1 MARCKS FCGR3A TNFRSF13B CLC CNRIP1 TPSAB1
E
Cluster 5
natural killer cell 73.54%
CD16-positive CD45-dim natural killer cell, human 11.01%
mature natural killer cell 4.04%
Cell type impact score
natural killer cell CL:0000623
mature natural killer cell CL:0000824
CD16−positive, CD56−dim natural killer cell, human CL:0000939
G
overall
bone marrow CITE−seq
bone marrow AbSeq
immune system
Accordion 75.8 87.9 70.2 72.1
scType 52.4 72.7 57 66.2
SCINA 50.3 33.3 47.9 35.4
ClustifyR 34.4 56.2 19.1 45.1
scCATCH 24.1 31.3 24.2 40
pancreas
liver
lung
kidney
Accordion 82.8 77 71.1 68.2
scType 38 30.5 42.2 49.8
SCINA 62.1 64.2 42.5 56.9
ClustifyR 0 (marker-CLASH!) 76.4 31.7 0 (marker-CLASH!)
scCATCH 10.4 22.9 17.9 13.1
Annotation performance (%)

Fig.3: The Cell Marker Accordion improves the annotation of cell types in multiple tissues from complex single-cell multiomics. *Annotation of single-cell datasets and interpretation of the results with the Cell Marker Accordion, and performance comparison with other marker-based annotation tools.* ***A*** *Dataset of PBMC FACS sorted cells separately profiled with single-cell RNA-seq. 15 surface antibodies were used to sort 10 different cell types, used as the ground truth. Populations identified by the Accordion are color-coded in the UMAP, with cluster numbers.* ***B*** *The Cell Marker Accordion annotation performance, measured as the similarity between the identified cell types and the ground truth (see* ***Methods****), is compared against other annotation tools.* ***C*** *Comparison of running times across annotation tools (time axis is log scaled).* ***D*** *Cell Marker Accordion interpretation of results: top three cell types achieving the highest impact score for each cell cluster (the winning cell type is highlighted).* ***E*** *Cell type annotation for cluster 5. Left: top three cell types, ordered according to their impact score, with corresponding percentages of cells in the cluster. Right: Cell Ontology tree of the top three cell types.* ***F*** *Top three marker genes with the highest impact score for each cell type, color-coded as* ***E****.* ***G*** *Comparison of annotation performances between the Cell Marker Accordion and other tools in multiple single-cell datasets from different tissues.*

Finally, to show the potential of the Cell Marker Accordion in annotating spatially resolved transcriptomics, we took advantage of a recently published adult mouse brain MERFISH dataset, with a panel of 1122 genes[48]. We considered a single brain coronal section, containing 37068 cells and 34 annotated cell types, used as ground truth (**Fig.4A, Supplementary Fig.5**). First, we performed cell type annotation with the Cell Marker Accordion (**Fig.4B**). Notably, the spatial mapping of the identified cell types revealed high similarity with the original annotation (**Fig.4C**). Also in the spatial scenario, the Cell Marker Accordion annotation performance improved by over 13% compared to the other tools (**Fig.4D,** see **Methods** and **Supplementary Data 3**).

Overall, these benchmarking results highlight the Cell Marker Accordion as a novel tool to obtain fast, more robust, consistent and highly interpretable annotation of cell populations in single-cell and spatial data.

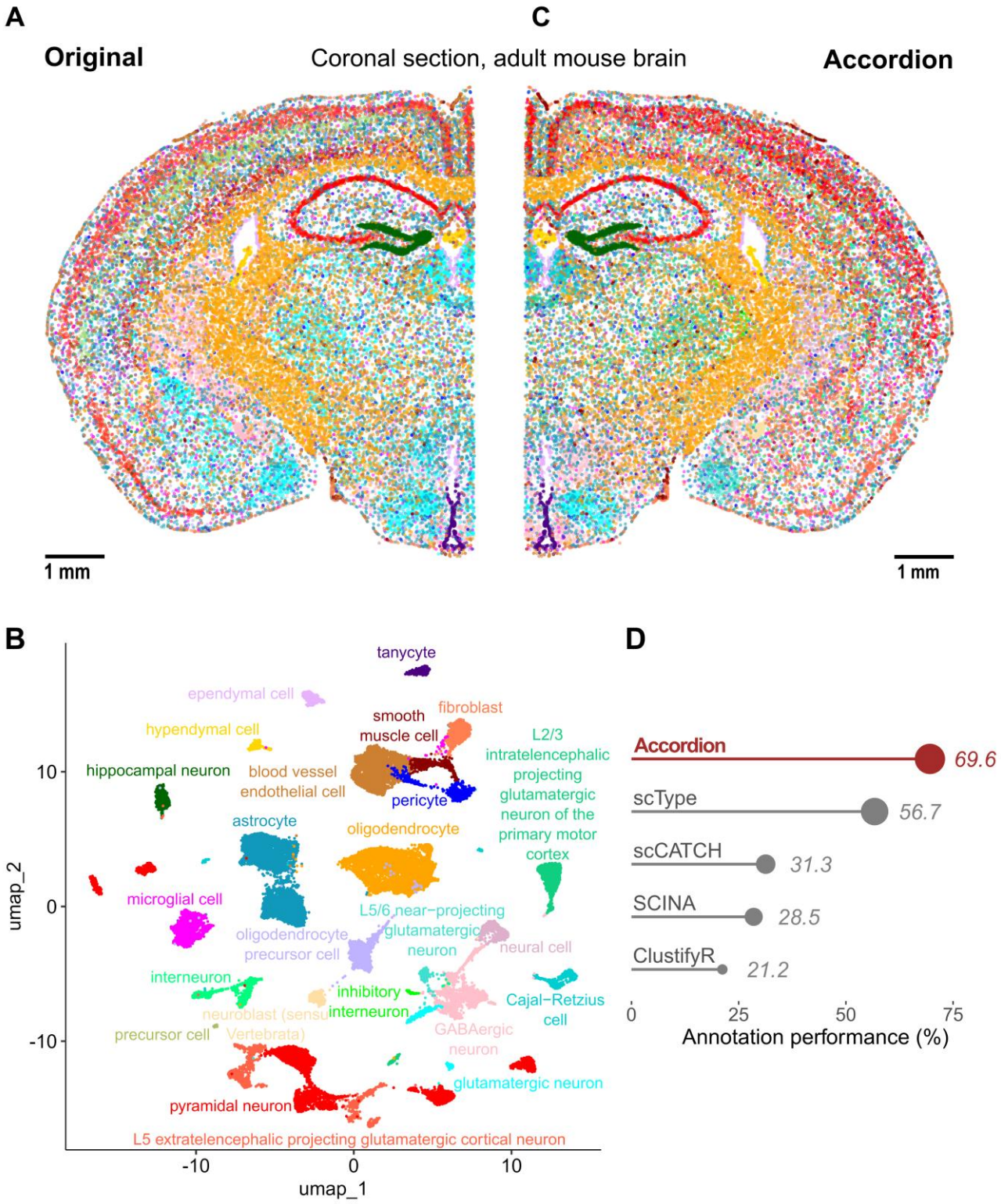

Fig.4: The Cell Marker Accordion improves the annotation of brain cell types in spatial transcriptomics. A *Spatial map and original annotation of a coronal section of an adult mouse brain, analyzed by MERFISH, based on a panel of 1122 genes[48]. Each dot corresponds to a cell, colored by cell type. Scale bar: 1 mm.* ***B*** *UMAP plot based on the transcriptional profile of each cell, with colors based on the annotation of the Cell Marker Accordion.* ***C*** *Spatial map with cells colored according to cell types as annotated by the Cell Marker Accordion. Scale bar: 1 mm.* ***D*** *Comparison*

across tools of annotation performances, measured as the similarity between predictions and ground truth.

The Cell Marker Accordion identifies disease-critical cells in human pathologies

Many pathologies, including tumors, contain critical cell populations exhibiting altered states and aberrant gene expression. These disease-critical cells significantly influence disease progression and treatment outcomes[20]. The persistence of a selective subset of malignant cells has been considered the underlying cause of the high relapse rates commonly observed in a variety of cancer patients[49–51]. Identifying and characterizing disease-critical cells in human pathologies is pivotal for improving diagnosis towards interceptive medicine[8], understanding pathogenesis and therapy resistance mechanisms, and developing novel therapies to specifically target and eradicate cancer-initiating cells while minimizing adverse effects on healthy cells. To expand the Cell Marker Accordion to the analysis of pathologies, we created a "disease" collection. We integrated marker genes associated with disease-critical cells found in multiple pathologies, including different tumor types affecting blood, brain, lung, pancreas and other tissues (**Fig.5A**). To obtain a standardized and consistent vocabulary of pathologies, we mapped disease terms to the Disease Ontology[52]

Notably, we collected more than 1073 markers associated with acute myeloid leukemia (AML), one of the most common types of blood cancer in adults[53]. A major challenge in AML treatment is the survival of a few therapy-resistant cells. Among these, leukemic hematopoietic stem cells (LHSCs) are key factors contributing to disease progression and relapse[20,49,54,55]. Therapy-resistant cells can show neoplastic monocytic features, associated with lower remission rates and overall survival[56–58]. To show the potential of the Cell Marker Accordion in identifying disease-critical cell types, we analyzed a published scRNA-seq dataset of CD34+ bone marrow cells from 5 healthy controls and 14 AML patients[59]. First, healthy cell types were annotated (**Fig.5B**). Next, by exploiting LHSC and neoplastic monocyte marker genes, the Cell Marker Accordion was able to assign an LHSC score and a neoplastic monocyte score for each cell (**Fig.5C,D**). Notably, we observed an accumulation of LHSCs in AML progenitor populations (**Fig.5C**), as well as an increase of neoplastic monocytes within AML monocyte-derived populations (**Fig.5D**). To extend our analysis to the context of therapies, we took advantage of another published scRNA-seq dataset of human bone marrow, with sequential samples at diagnosis and relapse from patients treated with the BCL-2 inhibitor venetoclax[57]. As for the previous dataset, we first annotated healthy cell types (**Fig.5E**). LHSCs and neoplastic monocytes were identified (**Fig.5F**, **Fig.5G**). Consistent with published results[27], we detected cells with high LHSC scores within progenitor populations and high neoplastic monocyte cell scores in monocyte-derived cells at diagnosis (**Fig.5F, Fig.5G**). At relapse, we observed the disappearance of LHSCs, implying that venetoclax-based treatment can target and eradicate them (**Fig.5F, Fig.5H**). Instead, neoplastic monocytes persisted after therapy, confirming, as previously proposed[57,60–62] , that the mechanism of resistance to venetoclax resides in an aberrant monocytic population (**Fig.5G, 5H**). These results suggest that malignant cell heterogeneity plays a significant role in treatment response and disease progression[20,61]. To further characterize the properties of leukemia aberrant cell types in AML patients, we extracted with the Cell Marker Accordion the top altered markers defining either LHSCs or neoplastic monocytes (**Fig.5I**).

We further demonstrated the potential of the Cell Marker Accordion in identifying disease-critical cells in single-cell datasets from patients with multiple myeloma (MM) (**Supplementary Fig.6**). We exploited a published scRNA-seq dataset of sorted bone marrow plasma cells from 11 healthy controls and 12 MM patients[63] (**Supplementary Fig.6A**). We identified neoplastic plasma cells with a significantly higher score in MM patients (**Supplementary Fig.6B,C**). These cells were clustered in patient-specific groups by the expression levels of specific immunoglobulin variable regions, suggesting distinct clonotypes (**Supplementary Fig.6D-G**). Importantly, the Cell Marker Accordion

was able to extract genes that are most critical for defining the identity of malignant plasma cells. (**Supplementary Fig.6F**).

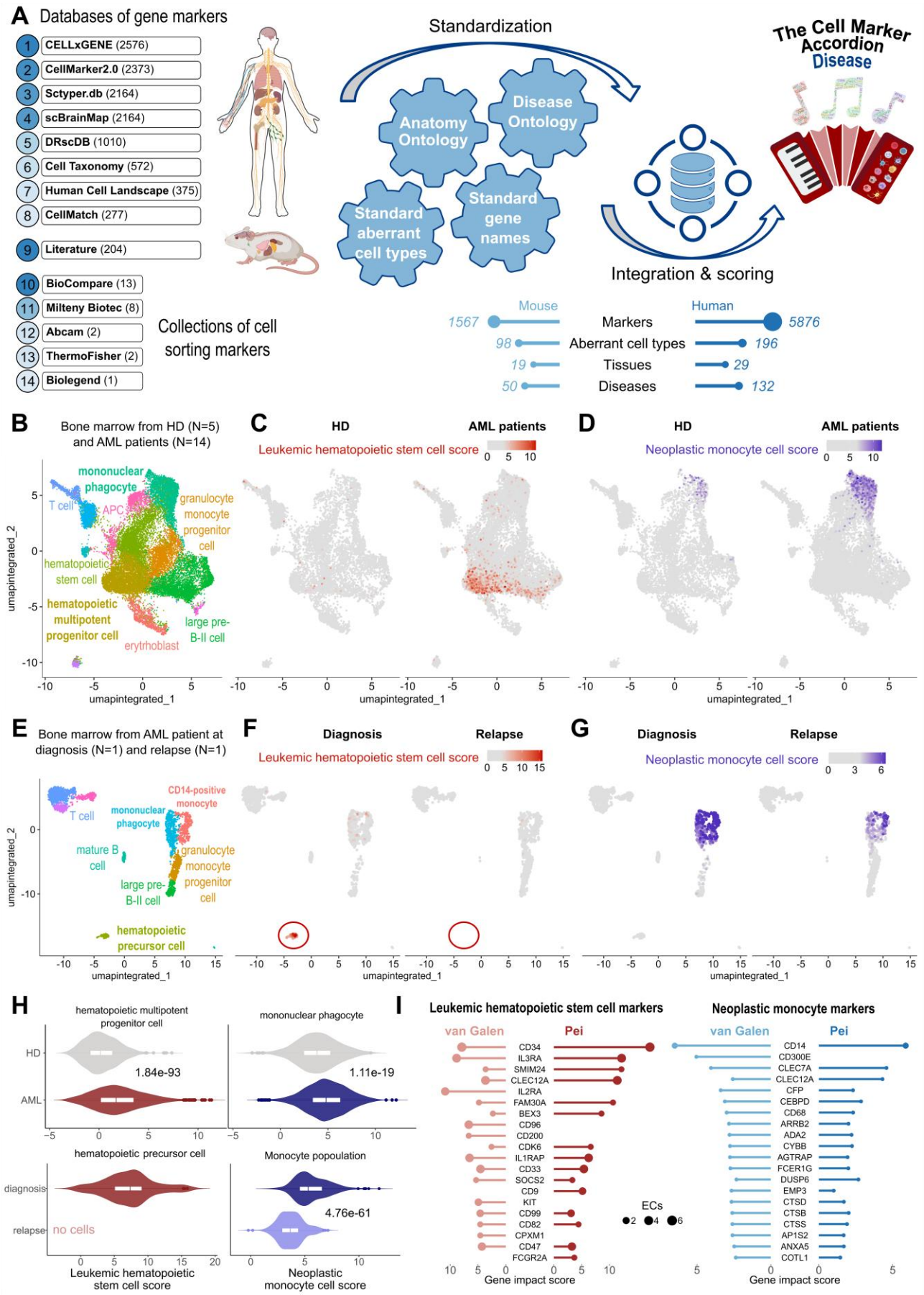
A
Databases of gene markers
1 CELLxGENE (2576)
2 CellMarker2.0 (2373)
3 Sctyper.db (2164)
4 scBrainMap (2164)
5 DRscDB (1010)
6 Cell Taxonomy (572)
7 Human Cell Landscape (375)
8 CellMatch (277)
9 Literature (204)
10 BioCompare (13)
11 Milteny Biotec (8)
12 Abcam (2)
13 ThermoFisher (2)
14 Biolegend (1)
Collections of cell sorting markers
Standardization
Anatomy Ontology
Disease Ontology
Standard aberrant cell types
Standard gene names
Integration & scoring
The Cell Marker Accordion Disease
Mouse
Human
1567 Markers 5876
98 Aberrant cell types 196
19 Tissues 29
50 Diseases 132
B
Bone marrow from HD (N=5) and AML patients (N=14)
mononuclear phagocyte
T cell
APC
granulocyte monocyte progenitor cell
hematopoietic stem cell
hematopoietic multipotent progenitor cell
erytrhoblast
large pre-B-II cell
umapintegrated_1
umapintegrated_2
C
HD
AML patients
Leukemic hematopoietic stem cell score
D
Neoplastic monocyte cell score
E
Bone marrow from AML patient at diagnosis (N=1) and relapse (N=1)
CD14-positive monocyte
mononuclear phagocyte
T cell
mature B cell
granulocyte monocyte progenitor cell
large pre-B-II cell
hematopoietic precursor cell
F
Diagnosis
Relapse
Leukemic hematopoietic stem cell score
G
Neoplastic monocyte cell score
H
hematopoietic multipotent progenitor cell
mononuclear phagocyte
HD
AML
1.84e-93
1.11e-19
hematopoietic precursor cell
Monocyte popoulation
diagnosis
relapse
no cells
4.76e-61
Leukemic hematopoietic stem cell score
Neoplastic monocyte cell score
I
Leukemic hematopoietic stem cell markers
van Galen
Pei
CD34
IL3RA
SMIM24
CLEC12A
IL2RA
FAM30A
BEX3
CD96
CD200
CDK6
IL1RAP
CD33
SOCS2
CD9
KIT
CD99
CD82
CPXM1
CD47
FCGR2A
ECs
Gene impact score
Neoplastic monocyte markers
CD14
CD300E
CLEC7A
CLEC12A
CFP
CEBPD
CD68
ARRB2
ADA2
CYBB
AGTRAP
FCER1G
DUSP6
EMP3
CTSD
CTSB
CTSS
AP1S2
ANXA5
COTL1

Fig.5: The Cell Marker Accordion identifies disease-critical cell types in acute myeloid leukemia patients. A *Workflow for building the Cell Marker Accordion Disease database. The resulting number of human and murine markers for aberrant cell types associated with various diseases from multiple tissues is reported.* Mouse and human illustrations created in BioRender. Tebaldi, T. (2025) https://BioRender.com/x09w717. ***B*** *Cell Marker Accordion annotation of human bone marrow cells from healthy donors (HD) and acute myeloid leukemia (AML) patients*[59]*.* ***C-D*** *Identification of leukemic hematopoietic stem cells (LHSCs) (**C**) and neoplastic monocytes (**D**). Cells are colored according to the Cell Marker Accordion scores.* ***E*** *Annotation of human bone marrow cells from AML patients at diagnosis and relapse after venetoclax treatment* [57]*.* ***F-G*** *Identification of LHSCs (**F**) and neoplastic monocytes (**G**) in AML patients at diagnosis and relapse.* ***H*** *Distribution of LHSC scores in hematopoietic progenitors (left) and neoplastic monocyte scores in monocyte populations (right) comparing AML patients with healthy donors (top) and AML patients at diagnosis and at time of relapse after venetoclax treatment (bottom). One-tailed Wilcoxon Rank Sum test was used, P-values are displayed.* ***I*** *Comparison of marker genes with the highest impact in defining LHSCs and neoplastic monocytes in the two leukemia datasets, for hematopoietic progenitor cells and monocytes, respectively.*

We next compared the Cell Marker Accordion performance in identifying aberrant tumor populations with respect to two available tools, SCEVAN[64] and CopyKAT[65], which identify tumor cells through calling copy number variations (CNV). For our benchmark, we exploited two published single-cell RNAseq datasets of glioblastoma and lung adenocarcinoma patients[24,25]. In the glioblastoma dataset, malignant cells were identified based on the expression of a gene list provided by the original authors (see **Methods** and **Supplementary Fig.7**) and were subsequently used as the ground truth. The lung adenocarcinoma dataset already included a classification of tumoral cells, which was directly used as ground truth. Performance annotation was assessed using two metrics: the percentage of correctly annotated cells and the corresponding F1 scores (see **Methods**). The Cell Marker Accordion achieved the best performance, identifying 100% of the malignant cells in the glioblastoma patients, with an F1 score of 0.97 (**Fig.6A**,**B**). Additionally, the Cell Marker Accordion significantly outperformed the other tools in terms of speed (**Fig. 6C**). While SCEVAN required more than 6 hours and CopyKAT more than 7 days to complete the annotation task, the Cell Marker Accordion achieved this in less than 2 minutes (**Fig. 6C**; see **Methods**). Furthermore, while other tools can only distinguish malignant versus non-malignant cells based on inferred CNV signatures, a defining advantage of the Cell Marker Accordion is its ability to dissect aberrant sub-populations based on expression alterations. In the lung adenocarcinoma dataset, the Cell Marker Accordion not only improved the accuracy in classifying malignant cells with respect to SCEVAN and CopyKAT (0.84 vs 0.52 and 0.52 F1 scores, respectively), but was also the only tool able to identify a small subpopulation of endothelial cells with a neoplastic gene expression signature, in agreement with the original publication[25](**Fig.6D, Fig.6E**).

Overall, these results provide evidence for the potential of the Cell Marker Accordion to identify malignant and neoplastic cells with aberrant states in human pathologies and to investigate disease mechanisms by extracting altered gene signatures in the quest for biomarker discovery.

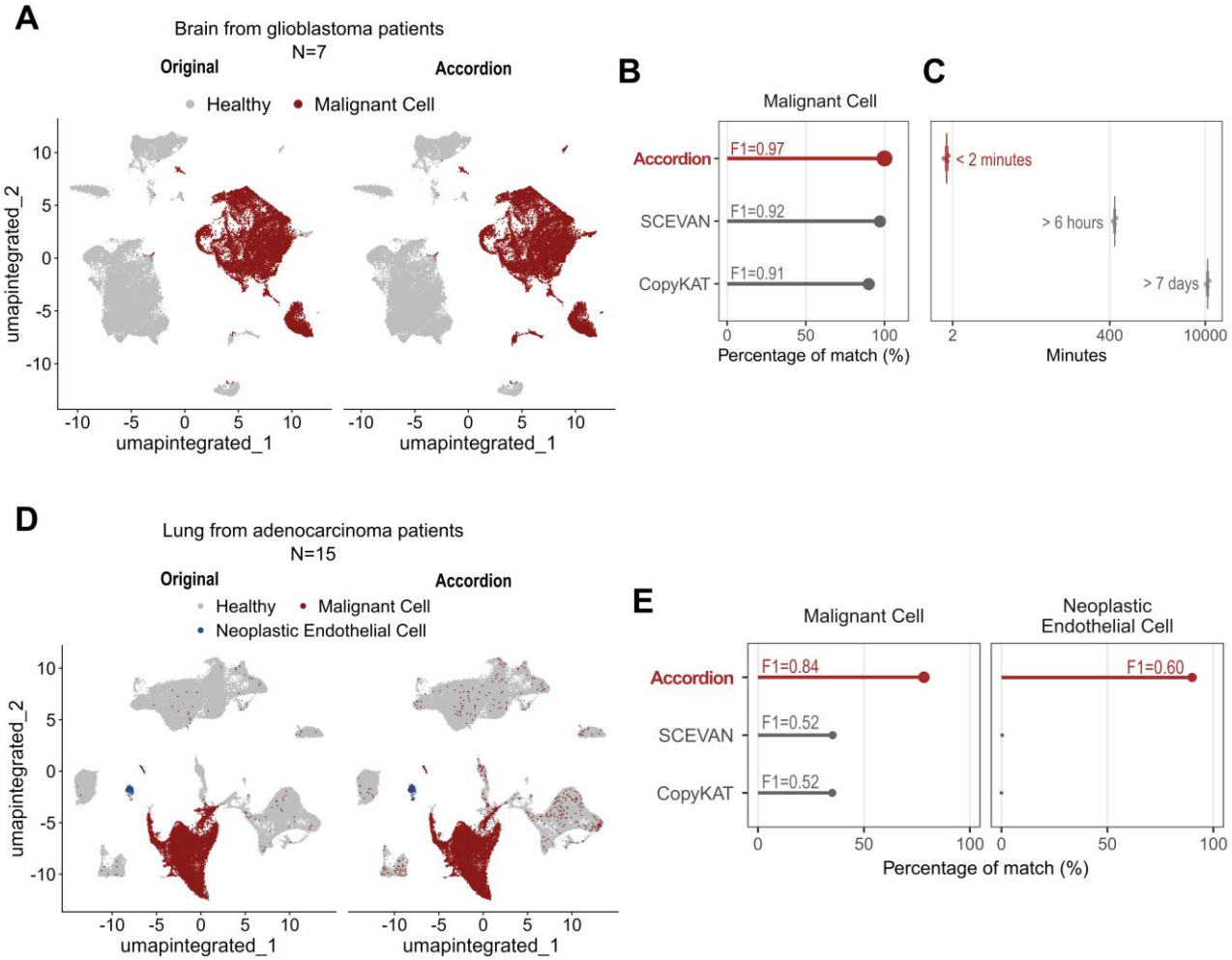

Fig.6: The Cell Marker Accordion improves the identification of malignant cells in solid tumors. A *Identification of malignant cells in glioblastoma patients. Left: original annotation[24]. Right: Cell Marker Accordion annotation.* ***B*** *Comparison of annotation performances in identifying glioblastoma malignant cells, measured as the percentage of cells corresponding to the ground truth and the relative F1 scores.* ***C*** *Comparison of annotation running times among tools.* ***D*** *Identification of malignant and neoplastic endothelial cells in lung adenocarcinoma. Left: original annotation[25]. Right: Cell Marker Accordion annotation.* ***E*** *Comparison of annotation performances in identifying malignant cells (left panel) and endothelial cells with a neoplastic gene expression signature (right panel).*

The Cell Marker Accordion identifies altered cell type composition in patients with splicing factor mutant myelodysplastic syndromes

Mutations in splicing factor (SF) genes are prevalent in approximately 50% of patients with Myelodysplasia (MDS) and Acute Myeloid Leukemia (AML)[66–68]. These mutations, especially the U2AF1 mutations, are linked to a high risk of AML transformation and decreased survival rates[69–75]. To explore the molecular mechanisms and biological implications that drive the clonal advantage of SF mutant cells over their wildtype counterparts, we conducted single-cell RNA sequencing on CD34+ cells from MDS patients, either without SF mutations (n=5) or with the U2AF1 S34F mutation (n=3). From a total of 62496 high-quality cells (see **Methods**), we identified cell types with the Cell Marker Accordion (**Fig.7A**). Most resulting cell types were related to blood progenitor cells, in line with the CD34+ cell sorting. To investigate the impact of the U2AF1 S34F splicing factor mutation, we compared cell type composition between U2AF1 WT and mutant patients (**Fig.7B**). Interestingly,

we observed an increase in hematopoietic multipotent progenitors, with a parallel decrease in erythroid lineage cells (**Fig.7B**). These results are consistent with the lineage-specific alterations induced by U2AF1 S34F, with impaired erythroid differentiation[27,76].

By single-cell mutation calling on reads mapping to the U2AF1 locus (see **Methods**), we classified each cell from U2AF1 S34F patient samples as either WT or S34F (**Fig.7C**). Notably, we observed that different cell types were characterized by various fractions of mutant cells, ranging from 5% to 32% (**Fig.7D**). This data confirm a myelo-monocytic shift with a reduction in megakaryocyte and erythroid lineage priming within hematopoietic stem and progenitor cells from patients with S34F mutant MDS (**Fig.7C**); accumulation of mutant cells within the megakaryocytic and erythroid lineage suggests a differentiation defect conferred specifically by the S34F mutation (**Fig.7D**).

Taken together, these results demonstrate that the Cell Marker Accordion can effectively identify and dissect cell-type variations driven by pathologically relevant mutations.

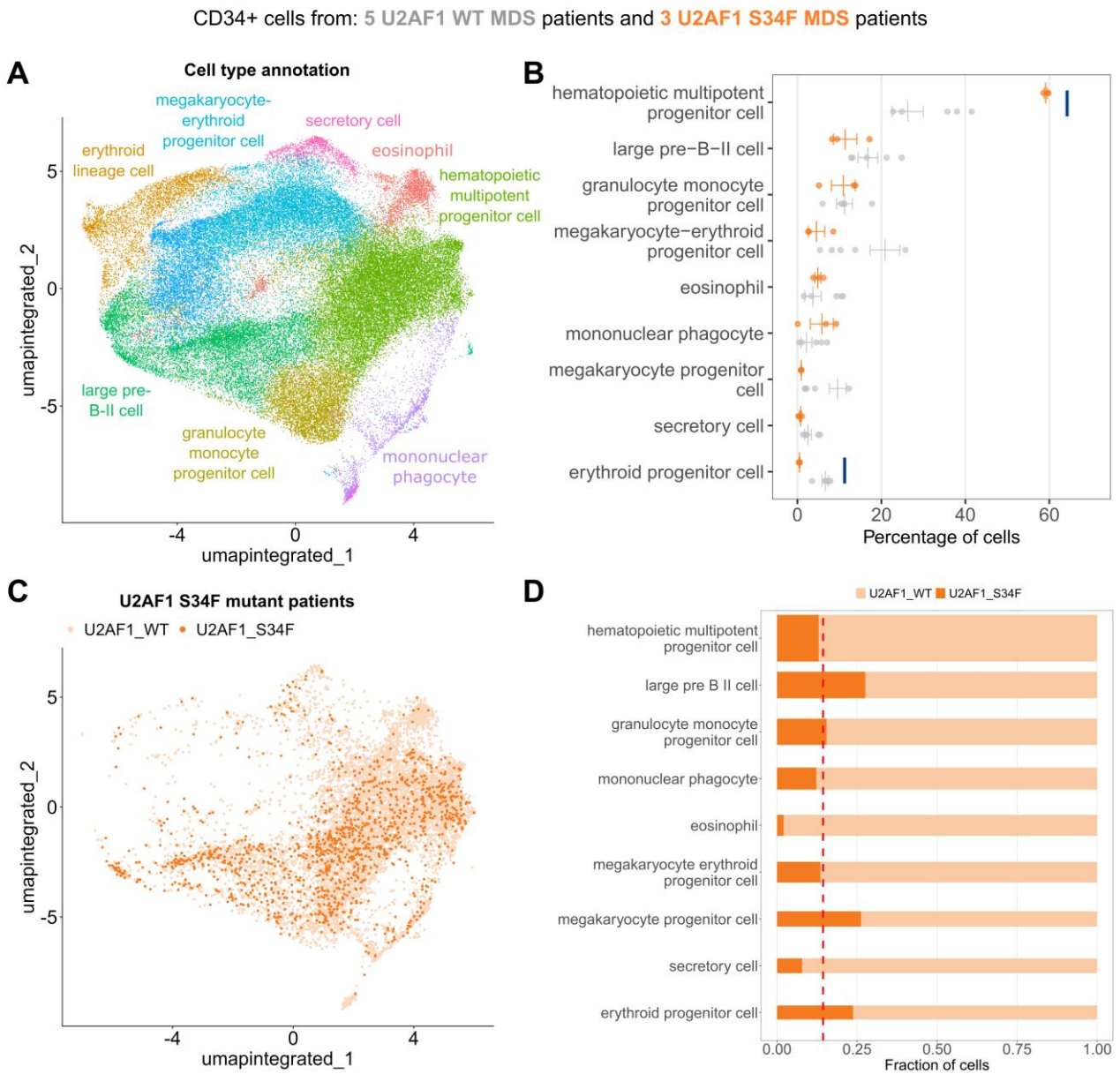

Fig.7: The Cell Marker Accordion identifies cell type alterations in splicing factor mutant cells from patients with myelodysplastic syndromes. ***A*** *Cell Marker Accordion cell type annotation of MDS patients with and without U2AF1 S34F mutation.* ***B*** *Changes in the abundance of hematopoietic cell types among conditions. Orange bars represent patients with U2AF1 S34F mutations, and grey bars represent patients without splicing factor mutations. Data are presented as mean values +/- SEM (U2AF1 WT, n=5, U2AF1 S34F, n=3). Compositional analysis was performed with the scCODA[77] python package based on Bayesian models. Credible and significant results are highlighted as blue bars, using an FDR threshold of 0.1.* ***C*** *Color-code representation of U2AF1 WT and S34F cells in S34F mutant patients.* ***D*** *Fraction of mutant (dark orange) and WT cells (light orange) within each cell type. The height of the bar is proportional to the average number of cells in each population. The dashed line represents the average number of mutant cells across all cell types in U2AF1 S34F patients.*

The Cell Marker Accordion identifies the activation of innate immunity pathways in mouse bone marrow

N6-methyladenosine (m6A) is the most abundant eukaryotic internal mRNA modification and significantly influences RNA biology[78–80]. This modification plays an important role in normal hematopoiesis, and alterations in m6A metabolism are strongly associated with acute myeloid leukemia pathogenesis, characterized by the overexpression of the m6A methyltransferase METTL3[81,82]. For this reason, pharmacological inhibition of METTL3 has been proposed as a therapeutic strategy to treat leukemias and other tumors[83].

To characterize the effect of m6A modulation on hematopoietic populations, we applied the Cell Marker Accordion to two murine single-cell datasets obtained from the bone marrow of Mettl3 conditional knockout mice[84] (**Fig.8A-D**) and from mice upon pharmacological inhibition of METTL3 with STM2457[85] (**Fig.8E-H**). After performing cell type annotation, we compared cell type compositions (**Fig.8B** and **8F**). In both datasets, we observed an increase in stem cells and megakaryocyte cells, together with a decrease in erythroid lineages upon Mettl3 deletion or inhibition (**Fig.8C** and **8G**). These observations are in line with the original publications and with results obtained in previous studies[28]. Next, we performed cell cycle annotation based on lists of cell-type phase-specific positive and negative markers (**Fig.8B** and **8F, right panels**). With this procedure, we could detect cell cycle changes in specific hematopoietic cell types, in particular, an increase of G0 cells among stem cells and megakaryocytes (**Fig.8D** and **8H**).

Two recent studies by us and others turned the spotlight on aberrant activation of innate immune pathways as a consequence of response to the deletion of the m6A methyltransferase Mettl3 or pharmacological inhibition, mediated by the formation of aberrant endogenous double-stranded RNAs[28,29]. To explore the impact of the knockout and the inhibition of Mettl3 on immunity in single-cell datasets, the Cell Marker Accordion computed an “innate immune response” score based on the activation of genes associated with this signature (**Supplementary Data 7**). Notably, both in the case of Mettl3 KO and drug-induced Mettl3 inhibition, we obtained a significant increase in the innate immune response score with respect to the control condition (**Fig.8I**). In addition, by extracting genes that mostly influence the immune response score, we found a subset that exhibits consistent activation in both murine models, as well as sets of genes that are specifically activated in response to either the knockout or the pharmacological inhibition of Mettl3 in murine hematopoietic stem and progenitor cells (**Fig.8J**).

Overall, these results demonstrate that the Cell Marker Accordion can be effectively used to characterize pathologically relevant pathways in disease or pharmacological treatment models.

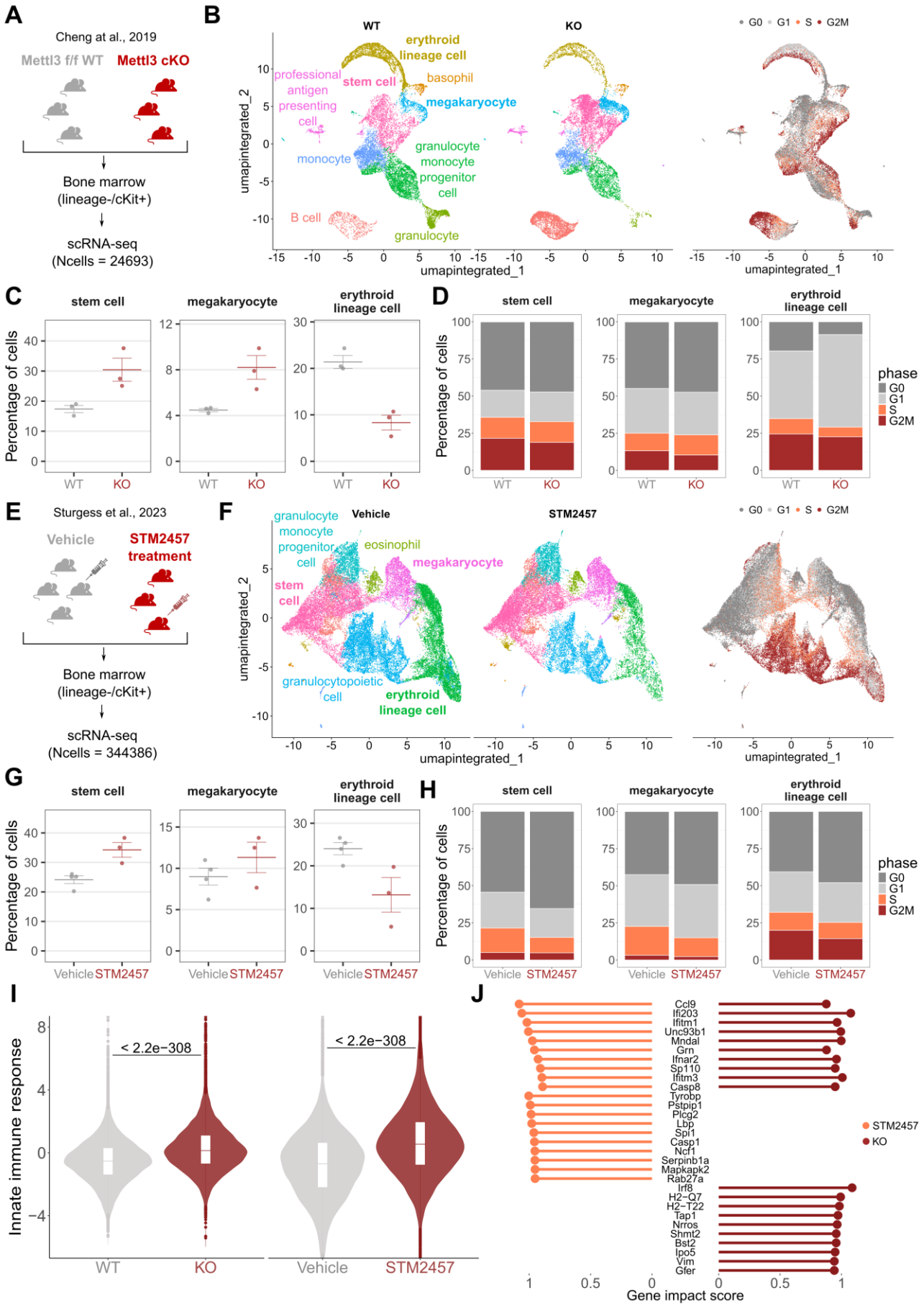
A
Cheng at al., 2019
Mettl3 f/f WT
Mettl3 cKO
Bone marrow
(lineage-/cKit+)
scRNA-seq
(Ncells = 24693)
B
WT
KO
G0 G1 S G2M
erythroid lineage cell
professional antigen presenting cell
stem cell
basophil
megakaryocyte
monocyte
granulocyte monocyte progenitor cell
B cell
granulocyte
umapintegrated_1
umapintegrated_2
C
stem cell
megakaryocyte
erythroid lineage cell
Percentage of cells
WT
KO
D
phase
G0
G1
S
G2M
E
Sturgess et al., 2023
Vehicle
STM2457 treatment
Bone marrow
(lineage-/cKit+)
scRNA-seq
(Ncells = 344386)
F
Vehicle
STM2457
granulocyte monocyte progenitor cell
eosinophil
megakaryocyte
stem cell
granulocytopoietic cell
erythroid lineage cell
G
H
I
Innate immune response
< 2.2e−308
< 2.2e−308
WT
KO
Vehicle
STM2457
J
Ccl9
Ifi203
Ifitm1
Unc93b1
Mndal
Grn
Ifnar2
Sp110
Ifitm3
Casp8
Tyrobp
Pstpip1
Plcg2
Lbp
Spi1
Casp1
Ncf1
Serpinb1a
Mapkapk2
Rab27a
Irf8
H2−Q7
H2−T22
Tap1
Nrros
Shmt2
Bst2
Ipo5
Vim
Gfer
STM2457
KO
Gene impact score

Fig.8: The Cell Marker Accordion identifies activation of innate immunity pathways in mice bone marrow. A *Schematic diagram of the single-cell experimental design of Cheng et al., 2019*[84] *dataset, comparing bone marrow from Mettl3 KO and WT mice.* ***B*** *Accordion cell types annotation of WT and KO mice and identification of cell cycle phase, based on lists of phase-specific markers.* ***C*** *Changes in the abundance of specific hematopoietic cell types upon Mettl3 KO. The increase in stem cells and megakaryocytes, with the parallel decrease of erythroid lineages, is consistent with literature.* ***D*** *Cell type-specific variations in cell cycle between WT and Mettl3 KO bone marrows.* ***E*** *Schematic diagram of the Mettl3 inhibition experimental design of Sturgess et al., 2023*[85] *dataset.* ***F*** *Accordion cell types annotation of mice treated with STM2457 METTL3 inhibitor and vehicle-treated mice, and identification of cell cycle phase.* ***G*** *Changes in the abundance of specific cell types between STM2457 and vehicle mice, consistent with changes observed in panel* ***C****.* ***H*** *Cell type-specific variations of the cell cycle between STM2457 and vehicle mice.* ***I*** *Significant increase of the "innate immune response" signature in Mettl3 KO and STM2457 treated cells, consistent with innate immunity activation observed in Gao et al., 2020* [28]*.* ***J*** *Genes involved in "innate immune response" pathways and showing the highest impact score in Mettl3 KO or STM2457 treated cells. One-tailed Wilcoxon Rank Sum test was used for panel* ***I****. P-values are displayed.*

Discussion

Accurate identification of cell types and states within heterogeneous and complex tissues is a prerequisite for comprehensive exploration and interpretation of single-cell and spatial data to provide biological insights. Yet, it is a challenging step in computational analysis workflows[10].

Here we present the Cell Marker Accordion, a user-friendly platform encompassing an interactive R Shiny web application and an R package designed to automatically identify and easily interpret single-cell populations in both physiological and pathological conditions. With respect to the majority of existing computational methods[12,17,19,38,41,64,65], the Cell Marker Accordion not only provides the user with an accurate annotation of cell types, but it is also able to detect disease-critical cells and pinpoint altered pathways in aberrant conditions, including cell cycle and quiescence analysis. The Cell Marker Accordion combines positive and negative markers, providing a more specific and unambiguous annotation. Cell types can be easily browsed following the Cell Ontology hierarchy and the Uber-anatomy ontology, to obtain the desired level of resolution. With respect to existing tools, the Cell Marker Accordion weights markers not only on their specificity but also on their consistency among resources, allowing a more robust cell type identification. Moreover, our tool allows the inclusion of customized annotations, by incorporating any weighted signature of interest. The biological interpretation of results is straightforward and unmatched by existing tools since the Cell Marker Accordion provides detailed information and graphics on genes, cell types or pathways that exert the most significant influence on annotation outcomes.

We validated the performance of the Cell Marker Accordion on 9 single-cell and spatial multi-omics datasets from different tissues, considering surface markers and expert-based annotations as a reference[42–47]. With no exception, the Cell Marker Accordion improved the identification of cell types compared to other available marker-based annotation tools[12,17,19,38,41,64,65], with an average increase of 23% in annotation performance. Additionally, the Cell Marker Accordion is remarkably faster than other tested tools, coupling high annotation accuracy with exceptional computational efficiency.

Accurate identification of cell types is also a fundamental requirement for investigating various pathologies, characterized by disease-critical cells with aberrant gene expression, playing a central role in disease progression and treatment response[20]. Identifying and characterizing disease-critical cells is pivotal for improving diagnosis and interceptive medicine [8], understanding pathogenesis and

therapy resistance mechanisms, identifying biomarkers, and developing effective therapies that minimize adverse effects on healthy cells. Current annotation tools focus mostly on physiological cell types. Some approaches, such as SCEVAN and CopyKAT, attempt to distinguish malignant cancer cells in single-cell RNA-seq through CNV calling but cannot be applied to pathologies with a minimal number of genomic alterations, such as leukemias[64,65]. To fill this gap, the Cell Marker Accordion includes weighted collections of marker genes associated with disease-critical cells in multiple common diseases, including solid and liquid tumors. By exploiting scRNA-seq datasets from multiple tumors, we showed that the Cell Marker Accordion effectively identifies aberrant cell types and extracts altered gene signatures, with improved specificity and lower running times than existing tools. While the Cell Marker Accordion's customizability suggests broad applicability in cancer and other diseases, our current benchmark, focused on two liquid and two solid tumors, demonstrates improved performance within these specific contexts. We plan to expand this benchmark in the future as the availability of high-quality, ground truth datasets increases.

Besides identifying disease-critical cells, the Cell Marker Accordion can be applied to the study and characterization of pathological processes. We demonstrated this in the context of myelodysplastic syndromes (MDS), where mutations in splicing factors (SF) genes such as U2AF1 are prevalent in approximately 50% of patients[66–68] and linked to decreased survival rates[69–75]. By applying the Cell Marker Accordion to single-cell data that we generated from bone marrow of a small cohort of MDS patients, we revealed skewing in the hematopoietic lineages in patients with U2AF1 S34F mutation. In particular, we observed impaired erythroid differentiation[27,76], pointing out the impact of a pathologically relevant splicing factor mutation on ineffective hematopoiesis and clonal advantage. This approach could be extended by tracking additional MDS mutations to determine their effect at various stages in differentiation.

Finally, we used the Cell Marker Accordion to dissect the effects of m6A RNA modification[78–80] and modulation of the METTL3 methyltransferase on hematopoiesis in murine models. Alterations in m6A have been strongly associated with acute myeloid leukemia pathogenesis[81,82], and pharmacological inhibition of METTL3 has been proposed as a therapeutic strategy[83]. The Cell Marker Accordion identified cell cycle changes and activation of immune response pathways in specific hematopoietic cell types, consistent with the formation of aberrant endogenous dsRNAs upon METTL3 depletion[28,29]. We extracted gene signatures activated in response to either the knockout or drug-mediated inhibition of METTL3 or both to demonstrate that the Cell Marker Accordion can be utilized to characterize pathologically relevant pathways in disease or pharmacological treatment models.

Complementary to the Cell Marker Accordion, several annotation tools exist that do not directly rely on marker genes[86,87]. These methods often rely on correlating reference expression data or transferring learned labels from other annotated single-cell datasets. However, these approaches necessitate high-quality and comprehensive reference datasets with annotated clusters for all relevant cell populations. Importantly, they can be susceptible to technical variations, such as differences in experimental platforms or sequencing strategies[14]. Given the current rate of evolution in single-cell and spatial omics technologies, this aspect cannot be underestimated. For this reason, a direct comparison between these approaches and the Cell Marker Accordion was not conducted in this study.

Fast-forward technological advances are expected to provide increasingly accurate and comprehensive measurements of single-cell and spatial populations. The Cell Marker Accordion is designed to accommodate updates and new sources of information, aiming for a more precise and refined cell type identification in diverse contexts and across different types of data. Possible

extensions of the Cell Marker Accordion include single-cell approaches profiling chromatin accessibility[88] or deconvolution of low-resolution spatial omics data.

In conclusion, the Cell Marker Accordion is a user-friendly, fast, flexible and powerful tool that can be exploited to improve the annotation and interpretation of single-cell and spatial datasets focused on studying diseases.

Methods

Data sources of the Cell Marker Accordion database

The Cell Marker Accordion database was constructed by considering multiple published marker gene databases and collections of cell-sorting markers in both physiological and disease conditions (**Supplementary Data 1**). Literature research was also conducted to collect additional marker genes associated with aberrant cell types for different diseases (each publication is considered a different source in calculating consistency scores). All annotation sources and references are reported in the Cell Marker Accordion database (https://rdds.it/CellMarkerAccordion).

We considered human and mouse marker genes associated with various tissues, including blood, bone marrow, immune system, pancreas, lung, liver, kidney and brain, along with their respective subtypes and associated diseases. Both positive and negative markers, when present, were selected. Marker genes' nomenclature was standardized to ensure the most recent approved version of gene symbols. HUGO Gene Nomenclature Committee (2024) and Mouse Genome Informatics (v. 6.24) resources were employed to standardize human and mouse gene names, respectively. To enable proper integration, we standardized original cell type labels among different sources by mapping them to the Cell Ontology (release 2024-08-16) (http://obofoundry.org/ontology/cl.html)[39], and the NCI Thesaurus OBO Edition (release 2024-05-07) (http://www.ebi.ac.uk/ols4/ontologies/ncit), for physiological and pathology associated cell types, respectively. The Uber-anatomy ontology (Uberon) (release 2024-09-03) (https://obofoundry.org/ontology/uberon.html)[40] was used to standardize tissue nomenclature. Finally, the Disease Ontology (release 2024-11-01) (https://disease-ontology.org/)[52] was exploited to standardize disease names.

After standardization and integration, Cell Marker Accordion includes a comprehensive collection of 15479 marker genes associated with 728 cell types in 212 human tissues, and 4118 marker genes associated with 493 cell types in 108 murine tissues (**Fig.2A**). Furthermore, the Cell Marker Accordion includes an extensive disease collection of 5876 genes associated with 196 aberrant cell types and 132 diseases in 29 human tissues, and 1567 genes associated with 98 aberrant cell types and 50 diseases in 19 murine tissues (**Fig.5A**).

Overlap among published marker gene databases

To quantify the overlap of marker genes between two marker gene databases (**Fig.1C**), we calculated the Jaccard pairwise similarity values. This was determined as the average Jaccard similarity of marker genes associated with common cell types present in both databases.

Definition of integration scores for marker genes in the Cell Marker Accordion database

After integration, the Cell Marker Accordion database describes each marker with a specificity score (SPs) and an evidence consistency score (ECs).

The SPs ranges from 0 to 1 and reflects how many cell types (CT) a gene (G) is a marker for. It is calculated separately for positive and negative markers as:

SPs_G = 1/Number of CT with *G* as a marker

A high SPs indicates that marker G is highly specific for a certain cell type, while a low SPs is associated with markers spread among multiple cell types.

The ECs evaluates the agreement of different annotation sources and measures marker robustness and reliability. It is calculated separately for positive and negative markers as:

$ECs_{G,CT}$ = Number of sources defining gene *G* as a marker of cell type *CT*

A high ECs indicates a high consensus of marker *G* among several sources and vice-versa.

Implementation of the Cell Marker Accordion R package for automatic annotation

The Cell Marker Accordion includes an R package to automatically identify cell type, cell cycle stage and pathway activation in single-cell and spatial omics data (https://github.com/TebaldiLab/cellmarkeraccordion). Users can annotate clusters or cells exploiting the built-in Cell Marker Accordion database with the *accordion()* function or can provide custom sets of markers using the *accordion_custom()* function. Both functions take as input a Seurat [34] object (versions 4 or 5) or a raw count matrix (**Supplementary Fig.1**). First, if no prior normalization and scaling steps have been performed, the single-cell expression matrix is normalized and scaled on input marker genes (SE, scaled expression). Based on the input, ECs are computed for each gene G and cell type CT, separately considering positive and negative markers. In case of conflicting sources, i.e. genes listed as positive and negative markers for the same cell type depending on the source, the ECs is penalized: ECs of negative occurrences are subtracted from ECs of positive occurrences to obtain the final ECs, whose sign will determine whether the marker is classified as negative (<0), positive (>0) or not considered (=0), and the final ECs is defined as the absolute value. ECs, ranging from 1 to 23 in the current Accordion database for both positive and negative markers, are log10 transformed to obtain regularized evidence consistency scores (ECs_reg) (**Supplementary Fig.1**). Next, the reciprocal of SPs is reverse scaled, separately for positive and negative marker. The result is then scaled to the same range of the ECs and log10 transformed, obtaining the regularized specificity score (SPs_reg). This procedure gives the same overall weight to the two scores. The resulting SPs_reg and ECs_reg are multiplied to obtain a final weight for each marker gene in each cell type. This final weight ranges from 1 to a maximum that depends on the marker database (5.6 in the current Accordion database, a magnitude similar to scaled gene expression levels). The scaled gene expression (SE) level is multiplied by this weight, obtaining a gene-weighted expression score, called gene impact score ($G_IMs_{G,C,CT}$), for each cell type (CT), each marker gene (G) in CT, in each cell (C):

$$G_IMs_{G,C,CT} = SE_{G,C} \times ECs_reg_{G,CT} \times SPs_reg_G$$

For each cell type, the normalized sum of all associated marker genes is calculated by summing, cell by cell, the weighted expression score divided by the square root of the weighted sum. This step leads to a *CT* x *C* enrichment score matrix, where rows represent cell types, columns represent cells and values indicate the associated cell type impact scores ($CT_IMs_{C,CT}$):

$$CT_IMs_{C,CT} = \frac{\sum_{G\epsilon PG} G_IMs_{G,C,CT}}{\sqrt{\sum_{G\epsilon PG} ECs_reg_{G,CT} \times SPs_reg_G}} - \frac{\sum_{G\epsilon NG} G_IMs_{G,C,CT}}{\sqrt{\sum_{G\epsilon NG} ECs_reg_{G,CT} \times SPs_reg_G}}$$

Where PG and NG are respectively positive and negative markers for the cell type CT. Each cell is then assigned to the cell type with the highest $CT_IMs_{C,CT}$. For annotating a cell cluster

(CC) the CC cell type impact score (CT_IMs_{CC}) is calculated, by default, as the third quartile of the distribution of the $CT_IMs_{C,CT}$ of cells belonging to CC:

$$CT_IMs_{CC,\,CT} = Q3_{C\epsilon CC}\, CT_IMs_{C,CT}$$

Each cell cluster is then assigned to the cell type with the highest $CT_IMs_{CC,CT}$, i.e the winning cell type (**Supplementary Fig.1**). When annotating cell clusters, the CC gene impact score (G_IMs_{CC}) is calculated by default as the third quartile of the distribution across all cells belonging to the same cluster. Additionally, at both cell and cluster annotation resolution, the cell type gene impact score is calculated, by default, as the third quartile of the $G_IMs_{G,C,CT}$ distribution across all cells belonging to the same winning cell type.

The Cell Marker Accordion Shiny app

The R Shiny tool is available at https://rdds.it/CellMarkerAccordion/. The Shiny app incorporates reactive programming allowing users to access the Cell Marker Accordion database and to retrieve marker genes that are specific for their selected cell types and tissues. Furthermore, when users choose genes of interest on the marker gene tab, the tool interactively retrieves the standardized cell types associated with the selected genes.

Validation of the Cell Marker Accordion

To validate the Cell Marker Accordion, we exploited eight single-cell and multi-omics datasets from different healthy tissues along with a spatial transcriptomic brain dataset (**Supplementary Data 4** and **Supplementary Methods**) For each dataset, the original cell type annotation was considered as ground truth. Cell type nomenclature was mapped to the Cell Ontology if necessary. After the preprocessing steps (see **Supplementary Methods),** each cluster was assigned to the cell type corresponding to the largest fraction of cells within the cluster. This approach ensures that the assignment reflects the predominant cell type composition within each cluster. Annotation performance was compared against five automatic annotation tools, ScType[38], SCINA[19], clustifyR[12], scCATCH[41], scSorter[17]. The Cell Marker Accordion was run using *max_n_marker* set to 30 and specifying the tissue of the dataset. All other tools were run using their default parameters (**Supplementary Data 5**). scType and scCATCH have in-built gene marker databases, which were used to run the tools. SCINA, clustifyR and scSorter require a user-provided set of marker genes in input: positive markers from the Cell Marker Accordion database were used in the benchmark. To avoid running failures, a maximum of 100 marker genes for each cell type was set for SCINA. For each tool, the annotation performance is measured as the average percentage similarity between the predicted cell type and the ground truth for each cluster. Percentage similarity between cell types is determined using the Cell Ontology tree and ranges from 0 to 100, where 0 represents the maximum possible distance, and 100 indicates a perfect match. This similarity was computed using the get_sim_grid function from the ontologySimilarity R package (version 2.7). Running time was also tested on the Zheng et al., 2017[42] dataset. To provide an unbiased comparison, we considered the same list of marker genes as input for all methods and ran the tools on the same machine three times. The benchmark was conducted on a server with: CPU: 2x Intel(R) Xeon(R) Gold 5318Y CPU @ 2.10GHz; RAM: 1536 GB DDR4. The tests were run on Ubuntu 22.10 with R v4.4.2. All tools were configured to use 4 threads. Running for over 3 hours without completion, scSorter was labelled with “Timeout” and excluded from further benchmarks.

To validate the Cell Marker Accordion on the annotation of disease-critical cells, we took advantage of two published single-cell datasets[24,25] of glioblastoma and lung adenocarcinoma patients samples.

In the glioblastoma dataset, tumor cell clusters were identified based on the expression of a gene list provided by the original authors, which included markers such as SOX2, OLIG1, GFAP, and S100B. We identified clusters 1,4,5,7,10,11,12,20,21 as tumor cells (**Supplementary Fig.7**) and used them as ground truth. The lung adenocarcinoma dataset was already annotated with malignant cell types, which were used as ground truth. Annotation performances were calculated as the percentages of correctly identified aberrant cells and the corresponding F1 scores, based on precision and recall. The Cell Marker Accordion performances and running times were compared against SCEVAN[64] and CopyKAT[65], run with default parameters (**Supplementary Data 5**).

MDS single-cell dataset

Human primary cells were obtained with patients' written consent after approval by the Yale University Human Investigation Committee. Bone marrow samples from MDS patients (**Supplementary Data 6**) were processed as previously reported in Biancon et al., 2022[89]. Briefly, viable (7-AADneg) CD34pos cells were sorted by the Yale Flow Cytometry facility on the FACSAria instrument (BD Biosciences) and subsequently processed for scRNA-seq library preparation by the Yale Center for Genome Analysis using Chromium Next GEM Single Cell 5' kit v2 (10x Genomics). A total of 64915 sequenced cells were used for downstream analysis, with an average of 71828 reads per cell and 3476 genes per cell. Variant detection at position 21:43104346-43104346 (U2AF1 S34F) was performed using FreeBayes v1.2.0 (https://github.com/freebayes/freebayes). Variant annotation was performed using VarTrix v1.1.19 (https://github.com/10XGenomics/vartrix). Single-cell expression data analysis was performed as described in **Supplementary methods**.

Data Availability

The Cell Marker Accordion gene marker database can be downloaded using the Shiny app at https://rdds.it/CellMarkerAccordion/. Sequencing files generated from patient samples (scRNA-seq) are available upon request. All publicly available scRNA-seq and spatial datasets used in this study are listed in **Supplementary Data 4.** A **Source Data** file is provided with this paper.

Data Access Guide

The Cell Marker Accordion curated database is available as an Excel file (**Supplementary Data 8**). Additionally, it is available in the GitHub repository of the Cell Marker Accordion Shiny web app (https://github.com/TebaldiLab/shiny_cellmarkeraccordion). The curated Cell Marker Accordion database can also be downloaded from the online Shiny web app (https://rdds.it/CellMarkerAccordion/) by clicking the "Download" button in the sidebar. The GitHub repositories for both the Shiny web app and the R package (https://github.com/TebaldiLab/cellmarkeraccordion) contain instructions on accessing and downloading the Cell Marker Accordion database.

The Cell Marker Accordion database can be easily explored or customized using the Shiny web app (https://rdds.it/CellMarkerAccordion/), which allows to: a) search and download lists of marker genes associated with input cell types across different tissues in health and disease; b) search and download lists of cell types associated with input marker genes across different tissues in health and disease; c) integrate custom set of marker genes with the Cell Marker Accordion database; d) perform cell type marker enrichment analysis across tissues in health and disease. Additionally, users can also browse hierarchies of cell types following the Cell Ontology structure in order to obtain the desired level of specificity in the markers and rank and select marker genes by their evidence consistency and specificity scores.

Demo examples are provided for guidance. All resulting tables can be easily explored and

downloaded. A tutorial to the web app's functionalities, along with instructions for local installation, is available on the GitHub page of the Shiny app: https://github.com/TebaldiLab/shiny_cellmarkeraccordion.

Code Availability

The Cell Marker Accordion R package, with code, tutorial and documentation, is available at: https://github.com/TebaldiLab/cellmarkeraccordion. To run the Cell Marker Accordion Shiny app locally the code is available at https://github.com/TebaldiLab/shiny_cellmarkeraccordion.

Acknowledgements

We thank Guilin Wang, Christopher Castaldi and the Yale Center for Genome Analysis for scRNA-seq guidance. We thank Lesley Devine and the Yale Flow Cytometry Facility for guidance in cell sorting. We thank all our patients and all clinical staff for their help with patient recruitment. We thank Emanuele Filiberto Rosatti and Roan Spadazzi for their valuable comments. This study was funded by AIRC under MFAG 2020 (ID. 24883 project) to T.T.. E.B. and T.T. were also supported by Fondazione VRT ("bando intelligenza artificiale 2024").
T.T. has been supported by MUR PNRR project CN RNA&GT RINGTAIL (CN00000041), M4C2 Inv 1.4, funded by the NextGenerationEU. S.H. was supported by NIH/NIDDK R01DK124788, NIH/NCI R01CA266604, NIH/NCI R01CA222518, NIH/NCI R01CA253981, U54DK106857, U01CA294514, The Frederick A. Deluca Foundation and the Edward P. Evans Foundation. G.B. was supported by AIRC under Start-Up 2023 - ID. 29035 project, the American Society of Hematology Scholar Award, and the Edward P. Evans Foundation. G.V. and F.L. were supported by the European Union within the MUR PNRR 'National Center for Gene Therapy and Drugs based on RNA Technology' (Project no. CN00000041 CN3 RNA). M.C.M. and V.B. were supported by AIRC IG 2021 no. 25704. This work was supported by the "Departments of Excellence 2023-2027" initiative (Law 232/2016), project no. 40613, funded by the Italian Ministry of University and Research (MUR), AIL Trento and AIL Bolzano.

Competing Interests

S.H., consultancy, Forma Therapeutics. Other authors declare no competing financial interests.

Authorship

Conceptualization: E.B., G.Bi., S.H. and T.T.; methodology: E.B., G.Bi., F.L., Z.I., G.V., S.H. and T.T.; investigation: E.B., G.Bi., I.C., K.R.A, J.V., T.S., S.H. and T.T.; formal analysis: E.B., G.Bi., I.C., F.L., Z.I., C.R., G.T., S.H. and T.T.; resources: S.H. and T.T.; validation: E.B., G.Bi., I.C., K.R.A, J.V, T.S., S.H., and T.T; writing: E.B., G.Bi., S.H. and T.T.; visualization: E.B., G.Bi., I.C., S.H. and T.T.; supervision: S.H. and T.T.; project administration: S.H. and T.T.; funding acquisition: S.H. and T.T.; revision: E.B., G.Bi., G.T., C.R., M.C., G.Bu., A.P., S.M.M., V.B., F.R., L.T., M.C.M., P.M., S.H. and T.T.

References

1. Monga, I., Kaur, K. & Dhanda, S. K. Revisiting hematopoiesis: applications of the bulk and single-cell transcriptomics dissecting transcriptional heterogeneity in hematopoietic stem cells. *Brief Funct Genomics* **21**, 159–176 (2022).

2. Wilson, N. K. & Göttgens, B. Single-Cell Sequencing in Normal and Malignant Hematopoiesis. *Hemasphere* **2**, e34 (2018).

3. Tian, Y. *et al.* Single-cell transcriptomic profiling reveals the tumor heterogeneity of small-cell lung cancer. *Signal Transduction and Targeted Therapy 2022 7:1* **7**, 1–16 (2022).

4. Walker, B. L., Cang, Z., Ren, H., Bourgain-Chang, E. & Nie, Q. Deciphering tissue structure and function using spatial transcriptomics. *Communications Biology 2022 5:1* **5**, 1–10 (2022).

5. Bressan, D., Battistoni, G. & Hannon, G. J. The dawn of spatial omics. *Science* **381**, eabq4964 (2023).

6. Lei, K. F., Ho, Y. C., Huang, C. H., Huang, C. H. & Pai, P. C. Characterization of stem cell-like property in cancer cells based on single-cell impedance measurement in a microfluidic platform. *Talanta* **229**, (2021).

7. Baslan, T. & Hicks, J. Unravelling biology and shifting paradigms in cancer with single-cell sequencing. *Nat Rev Cancer* **17**, 557–569 (2017).

8. Rajewsky, N. *et al.* LifeTime and improving European healthcare through cell-based interceptive medicine. *Nature 2020 587:7834* **587**, 377–386 (2020).

9. Abdelaal, T. *et al.* A comparison of automatic cell identification methods for single-cell RNA sequencing data. *Genome Biol* **20**, 1–19 (2019).

10. Pasquini, G., Arias, J. E. R., Schäfer, P. & Busskamp, V. Automated methods for cell type annotation on scRNA-seq data. *Comput Struct Biotechnol J* **19**, 961–969 (2021).

11. Ekiz, H. A., Conley, C. J., Stephens, W. Z. & O'Connell, R. M. CIPR: a web-based R/shiny app and R package to annotate cell clusters in single cell RNA sequencing experiments. *BMC Bioinformatics* **21**, 191 (2020).

12. Riemondy, K. A. *et al.* clustifyr: An R package for automated single-cell RNA sequencing cluster classification. *F1000Res* **9**, (2020).

13. Kiselev, V. Y., Yiu, A. & Hemberg, M. scmap: projection of single-cell RNA-seq data across data sets. *Nat Methods* **15**, 359–362 (2018).

14. Clarke, Z. A. *et al.* Tutorial: guidelines for annotating single-cell transcriptomic maps using automated and manual methods. *Nat Protoc* **16**, 2749–2764 (2021).

15. Wang, X., He, Y., Zhang, Q., Ren, X. & Zhang, Z. Direct Comparative Analyses of 10X Genomics Chromium and Smart-seq2. *Genomics Proteomics Bioinformatics* **19**, 253–266 (2021).

16. Wei, Z. & Zhang, S. CALLR: a semi-supervised cell-type annotation method for single-cell RNA sequencing data. *Bioinformatics* **37**, i51–i58 (2021).

17. Guo, H. & Li, J. scSorter: assigning cells to known cell types according to marker genes. *Genome Biol* **22**, 1–18 (2021).

18. Chen, Y. & Zhang, S. Automatic Cell Type Annotation Using Marker Genes for Single-Cell RNA Sequencing Data. *Biomolecules* **12**, (2022).

19. Zhang, Z. *et al.* SCINA: A Semi-Supervised Subtyping Algorithm of Single Cells and Bulk Samples. *Genes 2019, Vol. 10, Page 531* **10**, 531 (2019).

20. Stelmach, P. & Trumpp, A. Leukemic stem cells and therapy resistance in acute myeloid leukemia. *Haematologica* **108**, 353–366 (2023).

21. Thomas, D. & Majeti, R. Biology and relevance of human acute myeloid leukemia stem cells. *Blood* **129**, 1577–1585 (2017).

22. Frigyesi, I. *et al.* Robust isolation of malignant plasma cells in multiple myeloma. *Blood* **123**, 1336–1340 (2014).

23. Flores-Montero, J. *et al.* Immunophenotype of normal vs. myeloma plasma cells: Toward antibody panel specifications for MRD detection in multiple myeloma. *Cytometry B Clin Cytom* **90**, 61–72 (2016).

24. Abdelfattah, N. *et al.* Single-cell analysis of human glioma and immune cells identifies S100A4 as an immunotherapy target. *Nature Communications 2022 13:1* **13**, 1–18 (2022).

25. Kim, N. *et al.* Single-cell RNA sequencing demonstrates the molecular and cellular reprogramming of metastatic lung adenocarcinoma. *Nature Communications 2020 11:1* **11**, 1–15 (2020).

26. Shastri, A., Will, B., Steidl, U. & Verma, A. Stem and progenitor cell alterations in myelodysplastic syndromes. *Blood* **129**, 1586–1594 (2017).

27. Ganan-Gomez, I. *et al.* Stem cell architecture drives myelodysplastic syndrome progression and predicts response to venetoclax-based therapy. *Nature Medicine 2022 28:3* **28**, 557–567 (2022).

28. Gao, Y. *et al.* m6A Modification Prevents Formation of Endogenous Double-Stranded RNAs and Deleterious Innate Immune Responses during Hematopoietic Development. *Immunity* **52**, 1007-1021.e8 (2020).

29. Winkler, R. *et al.* m6A modification controls the innate immune response to infection by targeting type I interferons. *Nat Immunol* **20**, 173–182 (2019).

30. Oetjen, K. A. *et al.* Human bone marrow assessment by single-cell RNA sequencing, mass cytometry, and flow cytometry. *JCI Insight* **3**, (2018).

31. Hu, C. *et al.* CellMarker 2.0: an updated database of manually curated cell markers in human/mouse and web tools based on scRNA-seq data. *Nucleic Acids Res* **51**, D870–D876 (2023).

32. Franzén, O., Gan, L. M. & Björkegren, J. L. M. PanglaoDB: a web server for exploration of mouse and human single-cell RNA sequencing data. *Database* **2019**, 46 (2019).

33. Börner, K. *et al.* Anatomical structures, cell types and biomarkers of the Human Reference Atlas. *Nature Cell Biology 2021 23:11* **23**, 1117–1128 (2021).

34. Hao, Y. *et al.* Integrated analysis of multimodal single-cell data. *Cell* **184**, 3573-3587.e29 (2021).

35. Liberzon, A. *et al.* The Molecular Signatures Database (MSigDB) hallmark gene set collection. *Cell Syst* **1**, 417 (2015).

36. Abdulla, S. *et al.* CZ CELL×GENE Discover: A single-cell data platform for scalable exploration, analysis and modeling of aggregated data. *bioRxiv* 2023.10.30.563174 (2023) doi:10.1101/2023.10.30.563174.

37. Conde, C. D. *et al.* Cross-tissue immune cell analysis reveals tissue-specific features in humans. *Science* **376**, (2022).

38. Ianevski, A., Giri, A. K. & Aittokallio, T. Fully-automated and ultra-fast cell-type identification using specific marker combinations from single-cell transcriptomic data. *Nature Communications 2022 13:1* **13**, 1–10 (2022).

39. Diehl, A. D. *et al.* The Cell Ontology 2016: enhanced content, modularization, and ontology interoperability. *J Biomed Semantics* **7**, (2016).

40. Haendel, M. A. *et al.* Unification of multi-species vertebrate anatomy ontologies for comparative biology in Uberon. *J Biomed Semantics* **5**, 1–13 (2014).

41. Shao, X. *et al.* scCATCH: Automatic Annotation on Cell Types of Clusters from Single-Cell RNA Sequencing Data. *iScience* **23**, (2020).

42. Zheng, G. X. Y. *et al.* Massively parallel digital transcriptional profiling of single cells. *Nature Communications 2017 8:1* **8**, 1–12 (2017).

43. Stuart, T. *et al.* Comprehensive Integration of Single-Cell Data. *Cell* **177**, 1888-1902.e21 (2019).

44. Triana, S. *et al.* Single-cell proteo-genomic reference maps of the hematopoietic system enable the purification and massive profiling of precisely defined cell states. *Nature Immunology 2021 22:12* **22**, 1577–1589 (2021).

45. Jones, R. C. *et al.* The Tabula Sapiens: A multiple-organ, single-cell transcriptomic atlas of humans. *Science (1979)* **376**, (2022).

46. Guilliams, M. *et al.* Spatial proteogenomics reveals distinct and evolutionarily conserved hepatic macrophage niches. *Cell* **185**, 379-396.e38 (2022).

47. Sikkema, L. *et al.* An integrated cell atlas of the lung in health and disease. *Nature Medicine 2023 29:6* **29**, 1563–1577 (2023).

48. Zhang, M. *et al.* Molecularly defined and spatially resolved cell atlas of the whole mouse brain. *Nature 2023 624:7991* **624**, 343–354 (2023).

49. van Gils, N., Denkers, F. & Smit, L. Escape From Treatment; the Different Faces of Leukemic Stem Cells and Therapy Resistance in Acute Myeloid Leukemia. *Front Oncol* **11**, (2021).

50. Jongen-Lavrencic, M. *et al.* Molecular Minimal Residual Disease in Acute Myeloid Leukemia. *N Engl J Med* **378**, 1189–1199 (2018).

51. Ramos, A., Sadeghi, S. & Tabatabaeian, H. Battling Chemoresistance in Cancer: Root Causes and Strategies to Uproot Them. *Int J Mol Sci* **22**, 9451 (2021).

52. Baron, J. A. *et al.* The DO-KB Knowledgebase: a 20-year journey developing the disease open science ecosystem. *Nucleic Acids Res* **52**, D1305–D1314 (2024).

53. Shimony, S., Stahl, M. & Stone, R. M. Acute myeloid leukemia: 2023 update on diagnosis, risk-stratification, and management. *Am J Hematol* **98**, 502–526 (2023).

54. Hanekamp, D., Cloos, J. & Schuurhuis, G. J. Leukemic stem cells: identification and clinical application. *Int J Hematol* **105**, 549–557 (2017).

55. Barreto, I. V. *et al.* Leukemic Stem Cell: A Mini-Review on Clinical Perspectives. *Front Oncol* **12**, 931050 (2022).

56. Zhao, L. *et al.* Myelomonocytic and monocytic acute myeloid leukemia demonstrate comparable poor outcomes with venetoclax-based treatment: a monocentric real-world study. *Ann Hematol* **103**, 1197–1209 (2024).

57. Pei, S. *et al.* A Novel Type of Monocytic Leukemia Stem Cell Revealed by the Clinical Use of Venetoclax-Based Therapy. *Cancer Discov* **13**, 2032–2049 (2023).

58. Bruserud, Ø., Selheim, F., Hernandez-Valladares, M. & Reikvam, H. Monocytic Differentiation in Acute Myeloid Leukemia Cells: Diagnostic Criteria, Biological Heterogeneity, Mitochondrial Metabolism, Resistance to and Induction by Targeted Therapies. *Int J Mol Sci* **25**, 6356 (2024).

59. van Galen, P. *et al.* Single-Cell RNA-Seq Reveals AML Hierarchies Relevant to Disease Progression and Immunity. *Cell* **176**, 1265-1281.e24 (2019).

60. Kuusanmäki, H. *et al.* Phenotype-based drug screening reveals association between venetoclax response and differentiation stage in acute myeloid leukemia. *Haematologica* **105**, 708–720 (2020).

61. Beneyto-Calabuig, S. *et al.* Clonally resolved single-cell multi-omics identifies routes of cellular differentiation in acute myeloid leukemia. *Cell Stem Cell* **30**, 706-721.e8 (2023).

62. DiNardo, C. D. *et al.* Molecular patterns of response and treatment failure after frontline venetoclax combinations in older patients with AML. *Blood* **135**, 791–803 (2020).

63. Ledergor, G. *et al.* Single cell dissection of plasma cell heterogeneity in symptomatic and asymptomatic myeloma. *Nat Med* **24**, 1867–1876 (2018).

64. De Falco, A., Caruso, F., Su, X. D., Iavarone, A. & Ceccarelli, M. A variational algorithm to detect the clonal copy number substructure of tumors from scRNA-seq data. *Nature Communications 2023 14:1* **14**, 1–13 (2023).

65. Gao, R. *et al.* Delineating copy number and clonal substructure in human tumors from single-cell transcriptomes. *Nature Biotechnology 2021 39:5* **39**, 599–608 (2021).

66. Kennedy, J. A. & Ebert, B. L. Clinical Implications of Genetic Mutations in Myelodysplastic Syndrome. *J Clin Oncol* **35**, 968–974 (2017).

67. Visconte, V., Nakashima, M. O. & Rogers, H. J. Mutations in Splicing Factor Genes in Myeloid Malignancies: Significance and Impact on Clinical Features. *Cancers (Basel)* **11**, (2019).

68. Yoshida, K. *et al.* Frequent pathway mutations of splicing machinery in myelodysplasia. *Nature* **478**, 64–69 (2011).

69. Bejar, R. *et al.* Validation of a prognostic model and the impact of mutations in patients with lower-risk myelodysplastic syndromes. *J Clin Oncol* **30**, 3376–3382 (2012).

70. Graubert, T. A. *et al.* Recurrent mutations in the U2AF1 splicing factor in myelodysplastic syndromes. *Nat Genet* **44**, 53–57 (2011).

71. Ogawa, S. Genetics of MDS. *Blood* **133**, 1049–1059 (2019).

72. Patnaik, M. M. *et al.* Spliceosome mutations involving SRSF2, SF3B1, and U2AF35 in chronic myelomonocytic leukemia: prevalence, clinical correlates, and prognostic relevance. *Am J Hematol* **88**, 201–206 (2013).

73. Thol, F. *et al.* Frequency and prognostic impact of mutations in SRSF2, U2AF1, and ZRSR2 in patients with myelodysplastic syndromes. *Blood* **119**, 3578–3584 (2012).

74. Walter, M. J. *et al.* Clonal diversity of recurrently mutated genes in myelodysplastic syndromes. *Leukemia* **27**, 1275–1282 (2013).

75. Makishima, H. *et al.* Mutations in the spliceosome machinery, a novel and ubiquitous pathway in leukemogenesis. *Blood* **119**, 3203–3210 (2012).

76. Yip, B. H. *et al.* The U2AF1S34F mutation induces lineage-specific splicing alterations in myelodysplastic syndromes. *J Clin Invest* **127**, 2206–2221 (2017).

77. Büttner, M., Ostner, J., Müller, C. L., Theis, F. J. & Schubert, B. scCODA is a Bayesian model for compositional single-cell data analysis. *Nature Communications 2021 12:1* **12**, 1–10 (2021).

78. Desrosiers, R., Friderici, K. & Rottman, F. Identification of methylated nucleosides in messenger RNA from Novikoff hepatoma cells. *Proc Natl Acad Sci U S A* **71**, 3971–3975 (1974).

79. Frye, M., Harada, B. T., Behm, M. & He, C. RNA modifications modulate gene expression during development. *Science* **361**, 1346–1349 (2018).

80. Liu, N. *et al.* N(6)-methyladenosine-dependent RNA structural switches regulate RNA-protein interactions. *Nature* **518**, 560–564 (2015).

81. Nagy, R. M., Mohamed, A. A. E. H., El-Gamal, R. A. E. R., Ibrahim, S. A. M. & Pessar, S. A. Methyltransferase-like 3 gene (METTL3) expression and prognostic impact in acute myeloid leukemia patients. *Egyptian Journal of Medical Human Genetics* **23**, 1–13 (2022).

82. Li, M. *et al.* METTL3 mediates chemoresistance by enhancing AML homing and engraftment via ITGA4. *Leukemia 2022 36:11* **36**, 2586–2595 (2022).

83. Yankova, E. *et al.* Small-molecule inhibition of METTL3 as a strategy against myeloid leukaemia. *Nature* **593**, 597–601 (2021).

84. Cheng, Y. *et al.* m6A RNA Methylation Maintains Hematopoietic Stem Cell Identity and Symmetric Commitment. *Cell Rep* **28**, 1703-1716.e6 (2019).

85. Sturgess, K. *et al.* Pharmacological inhibition of METTL3 impacts specific haematopoietic lineages. *Leukemia 2023 37:10* **37**, 2133–2137 (2023).

86. Aran, D. *et al.* Reference-based analysis of lung single-cell sequencing reveals a transitional profibrotic macrophage. *Nature Immunology 2019 20:2* **20**, 163–172 (2019).

87. Lotfollahi, M. *et al.* Mapping single-cell data to reference atlases by transfer learning. *Nature Biotechnology 2021 40:1* **40**, 121–130 (2021).

88. Ranzoni, A. M. *et al.* Integrative Single-Cell RNA-Seq and ATAC-Seq Analysis of Human Developmental Hematopoiesis. *Cell Stem Cell* **28**, 472-487.e7 (2021).

89. Biancon, G. *et al.* Precision analysis of mutant U2AF1 activity reveals deployment of stress granules in myeloid malignancies. *Mol Cell* **82**, 1107-1122.e7 (2022).